THESIS

# USING ABOVE-GROUND DOWNWIND METHANE AND METEOROLOGICAL MEASUREMENTS TO ESTIMATE THE BELOW-GROUND LEAK RATE OF A NATURAL GAS PIPELINE.

Submitted by:

Fancy Cheptonui

Department of Systems Engineering

In partial fulfillment of the requirements

For the Degree of Master of Science

Colorado State University

Fort Collins, Colorado

Fall 2023

Master's Committee:

Advisor: Stuart N. Riddick
Co-Advisor: Daniel J. Zimmerle

Emily Fischer

ABSTRACT

USING ABOVE-GROUND DOWNWIND METHANE AND METEOROLOGICAL MEASUREMENTS TO ESTIMATE THE BELOW-GROUND LEAK RATE OF A NATURAL GAS PIPELINE.

Natural gas (NG) leaks from below-ground pipelines present a safety, economic, and environmental hazard, and triaging the severity of leaks remains a significant issue for pipeline operators. Typically, operators conduct walking surveys using hand-held methane ($CH_4$) detectors which output $CH_4$ concentrations to indicate the location of a leak, but quantification often requires excavation of the pipeline. Industry-standard $CH_4$ detectors are lower-cost and have a higher detection threshold and lower precision than optical-cavity $CH_4$ analyzers typically used to quantify emissions. It remains unclear whether coarser $CH_4$ concentration measurements could be used to identify the large leaks that require immediate response. To explore the utility of industry-standard detectors, above-ground downwind $CH_4$ concentration measurements made by the detectors as input to a novel modeling framework, the ESCAPE$^{-1}$ model were used to estimate the leak rates from below-ground NG pipelines. Controlled below-ground emission experiments were conducted to test this approach over a range of environmental conditions. Using 10-minute averaged $CH_4$ mixing/meteorological data and filtering out low wind/Pasquill Gifford Stability Class (PGSC) A events, the ESCAPE$^{-1}$ model estimates small distribution leaks (0.2 kg $CH_4$ $h^{-1}$) to within -31 to +75% (95% CI), and medium distribution leaks (0.8 kg $CH_4$ $h^{-1}$) to within -73 to +92%(95% CI) of the actual leak rate. When averaged over a longer period (more than 3 hours of data), the average calculated leak rate was an overestimate of 55% for the small (0.2 kg $CH_4$ $h^{-1}$)

leak and an underestimate of 6% for a medium distribution leak (0.8 kg $CH_4$ $h^{-1}$). Results suggest that as the wind speed increases, or the atmosphere becomes more stable both accuracy and precision of the leak rate calculated by the $ESCAPE^{-1}$ model decreases. This is likely the result of a trade-off between the high enough wind to move the gas but not high enough that the plume becomes collimated and less homogenous. Optimizing this approach for oil and gas industry applications, this study suggests that $CH_4$ mixing ratios measured by industry-standard $CH_4$ detectors lasting at least 3 hours could be used as a guide to prioritize NG leak repair by estimating the below-ground leak rate from a pipeline within reasonable uncertainty bounds (±55%) in favorable atmospheric conditions.

Key Words: Methane, Leak Detection, Leak Quantification, Pipeline Safety, Greenhouse Gases

# ACKNOWLEDGEMENTS

I am eternally grateful to Dr. Stuart Riddick for his support, teaching, and training throughout my master's program. For giving me feedback, for correcting me, and for ensuring that my thesis and publication are within the correct standard, thank you, Sir.

I am forever grateful to Prof. Daniel J. Zimmerle for giving me a chance to be his master's research student. Thank you for taking time out of your busy schedule to give me feedback on my project.

I am thankful to Prof. Emily Fischer for her feedback on my thesis, and for agreeing to be part of my master's committee.

I am grateful to UPSIDE/RPLUME project team members, Dr. Anna Hodshire, and the entire Zimmerle research group for their insightful feedback on my project.

I am indebted to my daughter, Glorianna Chemutai, my family, and friends in Kenya for believing in me.

Lastly, I thank the Clowney Memorial Fellowship, Department of Systems Engineering, and Mark Martinez & Joey Irwin Memorial Public Projects Fund through the Colorado Oil and Gas Conservation Commission (COGCC) for funding my master's and my research project.

# DEDICATION

I dedicate this to my daughter, Glorianna Chemutai, my sister, Miriam Chepkemoi, and My Family.

TABLE OF CONTENTS

LIST OF TABLES

LIST OF FIGURES

# 1 INTRODUCTION

## 1.1 Natural Gas in the US

In recent years natural gas (NG) has been used as an environmentally cleaner energy source compared to coal or oil as its combustion results in lower emission of greenhouse gas pollutants such as $CO_2$ (EIA, 2022), relative to coal or oil. The US production of NG in 2022 increased by 4% or 4.9 Bcf/d (averaging 119 Bcf/d) as compared to the production in 2021 (EIA, 2023). After production, NG is transported to processing plants for the removal of liquid hydrocarbons and impurities such as hydrogen sulfide and $CO_2$. Typically, pipelines are used to transport NG from production sites to the consumers. NG pipelines are classified into four categories: gathering pipelines, distribution pipelines, and transmission pipelines. Flowlines transport product from the wellhead to the wellpad, gathering lines transport NG products from the wellpad to processing plants, transmission pipelines transport refined NG across large distances, and distribution lines transport NG products to the consumer (EIA, 2023a).

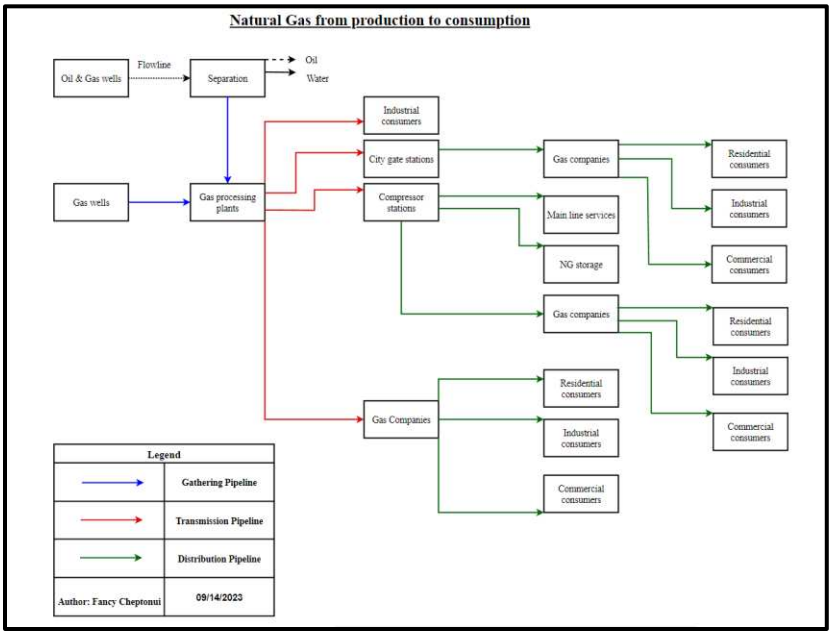


*Figure 1. NG transportation network from production to consumers.*

### 1.2 NG Pipeline leaks

Within the NG transportation system, pipeline damage can occur through corrosion, ground settlement, or excavation damage resulting in below-ground NG leaks and emission into the atmosphere. Despite its increased use as a cleaner fuel, NG is both a climate and public safety threat, consisting of between 70 and 90 % methane ($CH_4$) (Howard, 2015). Methane is a powerful greenhouse gas (GHG), with 28 times greater global warming potential than $CO_2$ over 100 years (IPCC, 2013), and is combustible when it collects to a concentration of between 5 and 15% in atmosphere with 26 % of oxygen in presence of a source of ignition. In 2021, $CH_4$ emissions from anthropogenic sources accounted for 12% of the total GHG emissions, of these, 23% came from oil and gas systems (U.S. EPA, 2023).

Recent studies suggest that $CH_4$ emissions from below-ground NG pipelines are a non-trivial source within the O&G system (Lowry et al., 2020). Several studies have reported on leak density and average emissions, Phillips et al. (2013) reported 4.3 leaks per mile of pipeline in Boston. Jackson et al. (2014) reported 3.9 leaks per mile of pipeline in Washington with emissions ranging from 0.3 to 0.9 kg $CH_4$ $h^{-1}$, and Weller et al. (2020) estimated a US national average of 0.5 leaks per mile of pipeline emitting 0.12 kg $CH_4$ $leak^{-1}$ $h^{-1}$.

### 1.3 NG Pipeline leak detection and quantification

The US regulates the distribution network through the Department of Transportation's Pipeline and Hazardous Materials Safety Administration (PHMSA). To mitigate leaks in the distribution network, PHMSA's Title 49 of the Code of Federal Regulations, Part 192 sets regulations governing pipeline safety, including regularly conducting pipeline inspections, leak detection, repair, and reporting of gas leaks (PHMSA, 2019). Generally, leak detection falls under walking and driving surveys. Leak quantification methods include flux chamber methods, high-flow sampling methods, and atmospheric dispersion modeling.

Under recent guidelines proposed by PHMSA(2023) addressing section 113 of the PIPES Act of 2020, distribution, Part 192-regulated gathering pipelines, and transmission pipelines should classify, and repair leaks based on the guidelines provided by GPTC.

Gas leaks are graded into three categories grades 1, 2, and 3. According to the Gas Piping and Technology Committee (GPTC, 2018), a grade 1 leak is a leak that requires immediate repair and continuous assessment to mitigate hazardous conditions. Any reading from inside a building, from an area near a transmission main, and from sub-surface structures (manholes or vaults) within 5 ft of a building that is ≥ 4 % of gas in the air is a grade 1 leak (GPTC, 2018). A grade 2 leak is, 1 any reading that is < 10 % of gas in air (within 30 ft of a building) on a paved area, 2 any reading that is ≥ 30 % of gas in air (within 50 ft of a building) on a paved area, 3 any reading < 20 % of gas in air (within 20 ft of a building) on an unpaved area, 4 any reading ≥ 10 % of gas in air (within 30 ft of a building) on a paved area, 5 any reading ≥ 20 % of gas in air (within 20 ft of a building) on an unpaved area, and 6 any reading that is ≥ 30 % of gas in air (within 50 ft of a building) on an unpaved area. A grade 2 leak should be inspected every 2 months and repaired within 12 months. Any reading that is less than 30 % of gas in the air within 50 ft of a building is a grade 3 leak.

Gas leak grading is based on both above-ground and below-ground gas reading levels and the distance to a nearby building. These gas reading levels change with environmental conditions such as wind speed and atmospheric stability (Riddick et al., 2021). In periods of increased wind speed and low atmospheric stability, there is an enhanced vertical transport within the near-surface atmosphere resulting in larger emission rates from the surface and lower observed surface concentration above a leak (Riddick et al., 2021).

### *1.3.1 Survey Methods*

To comply with regulations, NG pipeline operators use hand-held industry-standard instrumentation to detect gas leaks by conducting walking surveys. To conduct a walking survey,

an operator walks along a pipeline right of way while screening for above background $CH_4$ concentrations. Relatively low-precision instruments such as the Bascom-Turner Gas Rover (Measurement Range: 1 to 10,000 ppm, accuracy: ±2%), and the Remote Methane Leak Detector (RMLD; range: 0 to 99,9999 ppm-m; accuracy: ± 5 ppm-m) are used in a walking survey.

The Gas Rover draws air from an inlet typically pressed against the ground and measures the mixing ratio of $CH_4$ in the air sample in parts per million (ppm) or the percentage of gas, depending on the concentration of gas. The RMLD is a laser-based instrument and reports the line-averaged $CH_4$ mixing ratio along the laser path. When surveying a pipeline using an RMLD, the operator points the RMLD's laser at the suspected leak or across a suspected gas plume 15-30 m away (Heath, 2009). As the $CH_4$ detectors have relatively low precision and resolution, observations made during walking surveys are typically considered a binary indication of a below-ground leak and are not currently used to infer the size of a leak rate.

Driving surveys comprise an inlet mounted on a vehicle between 0.5 and 5 m above ground level (AGL), traveling between 4 and 11 m $s^{-1}$ (Von Fischer et al., 2017). The inlet is connected to a $CH_4$ analyzer capable of measuring $CH_4$ mixing ratios to parts per billion (ppb), such as the Picarro G2301 cavity ringdown spectroscopy gas analyzer (www.picarro.com ; measurement range: 0 to 20 ppm; precision: 1 σ over 5 s < 0.5 ppb; accuracy: ± 1 ppb over 24 hours). The major shortcomings of trace $CH_4$ analyzers are that they are typically more expensive than hand-held detectors and require either main power or batteries that only last a few hours.

### *1.3.2 Leak quantification methods*

Quantification of emission rate is more typically done during mobile surveys (Baillie et al., 2019; Jackson et al., 2014; Phillips et al., 2013; Von Fischer et al., 2017; Weller et al., 2020). The $CH_4$ analyzers used in mobile surveys have higher precision and lower detection thresholds than the detectors used in walking surveys, therefore, these can be used to quantify emissions when

measured concentrations and meteorological data are used as input in an atmospheric dispersion model. However, these instruments require specialist operators and are prohibitively expensive. Lower-cost leak quantification approaches such as the Hi-Flow sampler, or flux chamber methods exist. Flux chambers are classified into two types, Static and dynamic flux chambers. A flux chamber consists of an enclosure placed over the source of emission, for a static chamber, samples are drawn from the chamber at specific time intervals, every 5, 10, and 20 minutes (Kang et al., 2014). In a dynamic chamber, samples are taken from the chamber once a steady state is reached and maintained for approximately 10 minutes (Riddick et al., 2019). According to Riddick et al., (2019), it takes between 1 to 3 hours for a steady state to be reached and maintained for 10 minutes in a dynamic chamber. A gas chromatograph is used to measure the $CH_4$ concentrations in the samples from both the static and the dynamic chambers. The emission rate is calculated from the linear increase in $CH_4$ concentration over time (in a static chamber; Kang et al., 2014), or the steady-state (in a dynamic chamber; Riddick et al., 2019) $CH_4$ concentrations multiplied by the flow rate of air that is passed through the chamber.

A high-flow sampler is equipped with a surface enclosure, a catalytic & thermal conductivity hydrocarbon sensor, and a thermal gas flow sensor. When estimating the surface emission, the surface enclosure covers the emission area, the catalytic & thermal conductivity sensor measures $CH_4$ concentrations in the air stream, and the thermal gas flow sensor measures the sample flow rate (Lamb et al., 2015). The emission rate is derived by multiplying the $CH_4$ concentrations by the sample flow rate.

### *1.3.3 Atmospheric dispersion modeling*

Various atmospheric dispersion modeling approaches are used to quantify emissions from oil and gas equipment. The use of atmospheric dispersion modeling depends on the type of leak source. Generally, leak sources are classified into a point source, and an area source. In the oil and gas

industry, a point source is a single, localized, and distinguishable source of emission. An area source is a source that covers a large area such as a field, an animal pen, and a pond (Crenna, 2006).

Common atmospheric dispersion models include the Gaussian plume model (Chen et al., 2020; Zannetti, 1990), backward (Tian et al., 2022; Gao et al., 2009), and forward Lagrangian stochastic (Cai et al., 2008; Shadwick et al., 2007) models. Gaussian dispersion models track gas particles from the source of emission to a receptor location while the backward Lagrangian stochastic (bLs) model tracks pollutants from the receptor location to the source of emission. The Gaussian model and the forward Lagrangian stochastic models are used to quantify emissions from point sources while the bLs model is used to quantify emissions from area sources.

# 2 LITERATURE REVIEW

The estimation of the below-ground leak size of a NG pipeline remains challenging to operators during leak assessment, classification, and repair prioritization. NG pipeline operators rely on above-ground and below-ground concentration measurements to infer the size of a below-ground leak; however, these measurements change with atmospheric conditions such as wind speed, and atmospheric stability.

## 2.1 Classification of Atmospheric Stability

Atmospheric stability is the tendency of the atmosphere to resist or aid vertical motion of air particles. There are various ways of estimating atmospheric stability including the Monin-Obukhov length, temperature gradient, and bulk Richardson number (Mohan, 1998). These methods classify the mean state of the atmosphere and can be compared with the Pasquill classification system. Pasquill-Gifford Turner classification system classifies the atmosphere into PG (Pasquill Gifford) stability classes A to G that correspond to extremely unstable to extremely stable atmospheric conditions (Pasquill, 1961; Mohan, 1998).

Generally, in stable atmospheric conditions, the dry adiabatic lapse rate is greater than the environmental lapse rate; therefore, a parcel of unsaturated air is cooler than its environment (Nugent & Decou, 2018). The vertical motion is inhibited during stable conditions. In unstable atmospheric conditions, the dry adiabatic lapse rate is less than the environmental lapse rate; therefore, a parcel of saturated air is warmer than its environment (Nugent & Decou, 2018). Here, the vertical motion and mixing of particles is enhanced. Lastly, in neutral atmospheric conditions, the dry adiabatic lapse rate is the same as the environmental lapse rate; therefore, a parcel of air is

at the same temperature as its environment (Nugent & Decou, 2018). In neutral atmospheric stability, vertical motion of particles is neither aided nor resisted.

## 2.2 Previous leak rate estimation methods

### *2.2.1 Chamber methods*

Various studies have used flux chamber methods, high-flow sampling units, and atmospheric dispersion modeling to estimate emissions from below-ground NG pipelines. Lamb et al., (2015, 2016) report on estimating emissions from below-ground pipelines using a high-flow sampling unit. Air is flushed through the sampling unit's chamber and concentrations are measured once a steady state is reached. Here, the leak rate is estimated based on the concentrations. The shortcomings of this method are that it is time-consuming as it takes up to 3 hours for a steady state to be reached, and it estimates emission based on a $1.2 \times 1.2$ $m^2$ surface enclosure. Studies by Cho et al. (2020) and Riddick et al. (2021) show that $CH_4$ flows up to a radius of 4.5 m on the surface. Therefore, estimating emissions based on a $1.2 \times 1.2$ $m^2$ enclosure might mean that the chamber is not capturing the entire surface flux. In addition, some studies used the chamber methods to cover the emission area in several steps. This technique might not be accurate as the emission from an area source changes exponentially. Also, Chamber methods are time-consuming as either the entire emission area must be enclosed by the chamber, or the leaking pipeline exposed to cover the leak.

Hendrick et al. (2016) utilized a flux chamber to estimate emissions from below-ground leaks in the NG distribution pipeline. Like the high flow sampling, chamber methods require the pipeline to be exposed or use of multiple measurement chambers. High-flow sampling and chamber methods share the shortcomings of time, being expensive and inconvenient if the leak is in an urban or suburban environment. In both an urban and a suburban environment, continuous, safe, and sustained access to an area might be restricted making it challenging to quantify leaks.

To date, no unobtrusive method uses available instrumentation to quantify the rate of a below-ground pipeline leak.

### *2.2.2 Atmospheric dispersion modeling*

A below-ground pipeline leak presents as an area source on the surface, this complicates the quantification and grading of pipeline leaks. For such leaks, some studies have used the bLs atmospheric dispersion model to estimate emissions. Atmospheric dispersion modeling relies on concentration data to estimate emissions from below-ground pipelines. Tian et al. (2022) report on the use of the backward Lagrangian stochastic (bLs) model to estimate emission from below-ground leaks to within 50% of a controlled release rate when 1 hour of data is used. Tian et al. (2022) suggest that a representative amount of data (3 – 4 hours of data) is required to accurately estimate emissions using the model. Other studies have proved useful in estimating trace gas emissions using the bLs model ( Flesch et al., 2005; 2004; Flesch & Wilson, 2005).

## 2.3 Research objectives

Despite NG leaks being both a safety and an environmental concern, there is currently no way to quickly estimate the size of the below-ground leak rate and effectively prioritize leaks for repair. Leak detection methods use instrumentation that reports $CH_4$ mixing ratios in ppm but are not currently used for emission quantification. Further, current methods of leak classification do not consider the effect of weather conditions and atmospheric stability of above-ground $CH_4$ concentrations. This study aims to investigate whether $CH_4$ mixing ratios from an industry-standard instrument can be used to infer a pipeline's below-ground gas leak rate. Specifically, the objectives of this study are to:

1. Estimate the surface $CH_4$ emission rate using $CH_4$ mixing ratios and meteorological data, and thereafter derive the below-ground leak rate.
2. Assess the accuracy of this approach by comparing estimated leak rates with the controlled release rates in different environmental conditions and atmospheric stabilities.
3. Determine the meteorological conditions and atmospheric stabilities where this approach works best.

# 3 METHODS

Experiments were conducted at the Methane Emissions Technology Evaluation Centre (METEC), a facility under Colorado State University's Energy Institute. Currently, METEC has several testbed configurations that allow for controlled release of NG to simulate gas leaks in below-ground pipelines. Two of the testbeds allow for controlled release of gas under varied below-ground and surface conditions hence simulating a rural environment (vegetation covered: rural testbed) or an urban/suburban environment (asphalt covered: urban testbed). Gas leaks in both testbeds can be released at varying leak rates and leak depths. Various leak detection and quantification methods can be tested at the testbeds. Detailed descriptions of both rural and urban testbed designs can be found in Jayarathne et al. (2022). Although METEC has different testbeds with different configurations and sub-surface properties, above-ground measurements in this study were taken from the rural testbed.

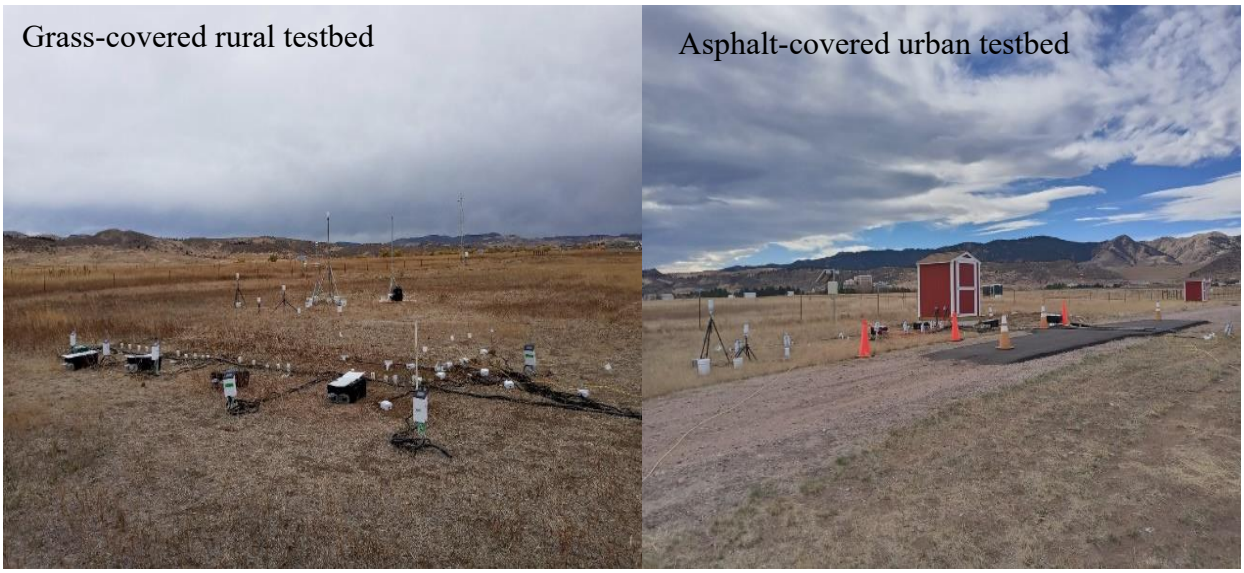


*Figure 2. METEC testbeds. a.) shows the rural testbed, and b.) shows the asphalt covered urban testbed.*

### 3.1 Below-ground controlled release of NG

Gas was supplied to the below-ground release point from compressed NG cylinders (containing 85 % - 95 % $CH_4$) through a thermal mass flow meter that was calibrated with nitrogen of known flow rate. The flow rate is controlled by solenoid valves and precision orifices, while gas chromatography is used to measure the $CH_4$ content of NG in the controlled release gas.

The rural testbed comprises a permeable (grass) surface cover with leak depths of 0.6 m, 0.9 m, and 1.8 m (Jayarathne et al., 2022). Using the 0.9 m leak depth, a PTFE (Polytetrafluoroethylene) tubing with a diameter of 6.35 mm (model SS-MD-4, Swagelok, USA) was installed below the ground to simulate a buried pipeline gas leak. The buried end of the tubing was capped with a 3 μm filter, covered using gravel to avoid soil packing, then backfilled with the local soil.

Controlled release rates were set at 0.2, 0.4, and 0.8 kg $h^{-1}$ (Table 1) for different experiments to investigate small to medium pipeline leaks (Hendrick et al., 2016; Lamb et al., 2015; Weller et al., 2018). Large distribution leaks, greater than 1 kg $CH_4$ $h^{-1}$ (Hendrick et al., 2016; Lamb et al., 2015; Weller et al., 2018) were not tested due to concerns about damaging the test bed. Gas was released 24 hours before each experiment to establish a steady state flow between the leak point and the surface. Studies by Mitton (2018), and (Tian et al., 2022) show that a steady state can be achieved in approximately 4 hrs for the selected leak rates. According to Gao et al. (2021), a steady-state gas flow at the testbeds is shown by a negligible change in surface concentration at the point that is situated directly above the below-ground leak point.

*Table 1. Experiments that were conducted at Colorado State University's METEC facility to test the performance and accuracy of the modeling approach in estimating below-ground leak rates. The table shows the controlled release rates, duration of the experiments (in hours), $CH_4$ mixing ratios (averaged over the duration), wind speed (in m $s^{-1}$), and PGSC (Pasquill Gifford Stability Class).*

| Exp No. | Controlled Release Rate (kg $h^{-1}$) | Duration (hrs) | $CH_4$ mixing ratio. (ppm-m) | Wind speed (m $s^{-1}$) | PGSC |
|---|---|---|---|---|---|
| 1 | 0.2 | 6 | 73 | 2.6 | B |
| 2 | 0.4 | 6 | 83 | 1.3 | B |
| 3 | 0.4 | 3 | 89 | 3.4 | D |
| 4 | 0.4 | 6 | 89 | 2.1 | B |
| 5 | 0.4 | 4 | 85 | 1.2 | A |
| 6 | 0.4 | 5 | 75 | 1.8 | A |
| 7 | 0.8 | 4 | 73 | 1.0 | A |
| 8 | 0.8 | 3 | 109 | 2.0 | C |

**3.2 Above-ground methane measurements**

Above-ground measurements were taken from the 'rural testbed' at METEC between 27 September to 3rd December 2021. All above-ground $CH_4$ mixing ratios were measured every 2 seconds using the intrinsically safe version of the Remote Methane Leak Detector, henceforth referred to as the RMLD (Health Consultants Inc, Texas, USA). The RMLD is an open path Tunable Diode Laser Absorption Spectrometer (TDLAS) that reports line-averaged $CH_4$ mixing ratios in parts per million-meter (ppm-m). The RMLD's laser unit was mounted at 2 m AGL during an experiment.

A reflective screen was set up directly opposite the laser, between 10 and 20 m away. The laser/screen set was positioned at a downwind distance of 10 m from the source. The laser path was set perpendicular to the wind direction (Figures 3 and 4). One advantage of using a line-averaging sensor is that it makes it possible to survey a location from a distance (Heath, 2009), this is useful in areas where the leak location is inaccessible.

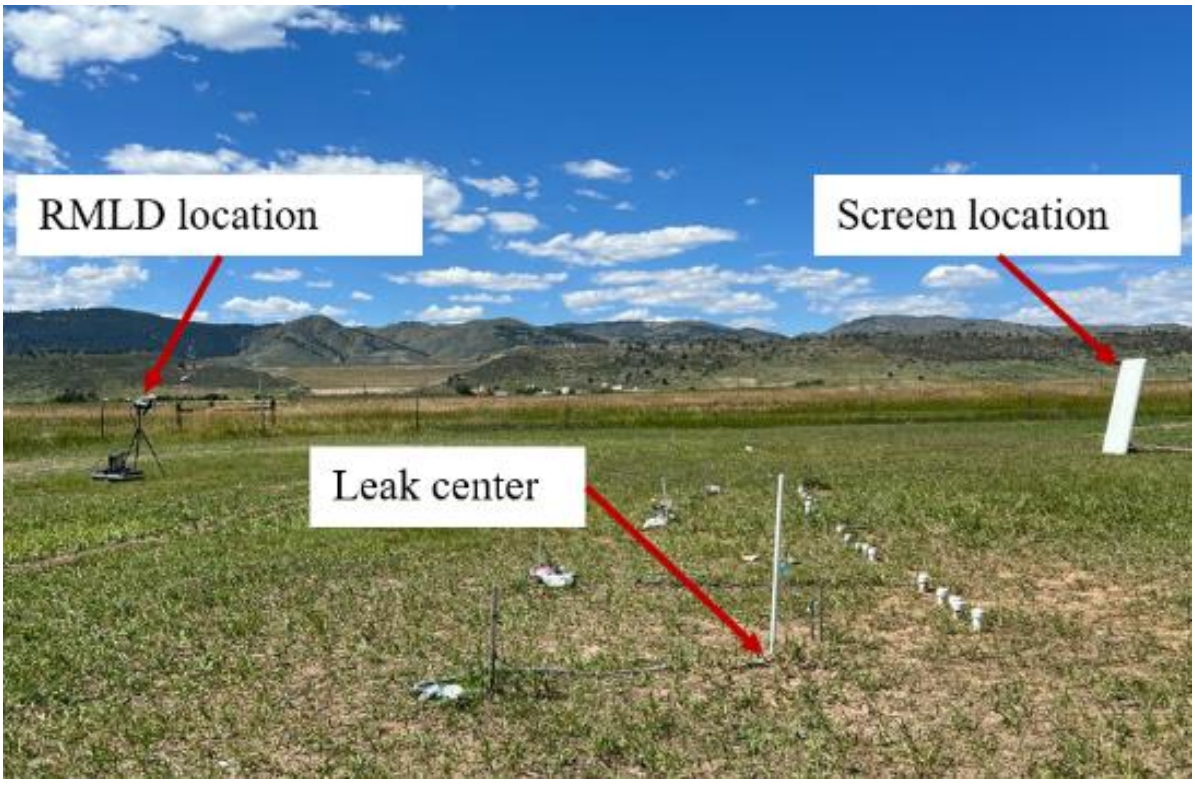


*Figure 3. Above-ground setup during an experiment. The reflective screen was set directly opposite the RMLD laser (installed 2 m AGL), and the combination was set 10 - 20m downwind of the leak center.*

Before each measurement period, the RMLD was self-tested ((Heath, 2009); Section A2.2). A self-test is done by removing the controller from the carrying case, turning on the RMLD, and allowing it to warm up for 2 to 3 minutes. Considering that the RMLD is used by oil and gas operators to detect leaks and is not routinely used for accurate quantification of leak rates, a Picarro G4302 Gas Scouter (Picarro Inc, California, USA; Precision: 3 ppb in 1 sec) was used to validate the $CH_4$ mixing ratios. For validation (Figure A2), $CH_4$ mixing ratio measurements were sampled side-by-side using both the RMLD and the Picarro.

### 3.3 Meteorological measurements

Meteorological data, including wind speed, wind direction (º East of North), relative humidity, and air temperature, were measured by a sonic anemometer (Model 81000, R. M. Young Co. Michigan). The sonic anemometer is installed 6 m AGL and located 20 m West and 50 m North of the leak center. Since meteorological data were recorded at 6 m AGL, wind speed was corrected to 2 m to match the measurement height of $CH_4$ using Equation 1. Wind speed at 2 m AGL ($WS_2$, m $s^{-1}$) is calculated as a function of the wind speed at 6 m AGL ($WS_6$, m $s^{-1}$), the heights AGL ($h_2$, and $h_6$, both m), the zero-plane displacement (d, m), and the surface roughness length ($z_0$, m) in meters (Hadi, 2015). The $z_0$ was set at 0.023 m and d at 0.04 m to represent the short grass cover on the testbed (Seinfeld & Pandis, 2016).

$$WS_2 = WS_6 \times \frac{\ln(\frac{h_2 - d}{Z_0})}{\ln(\frac{h_6 - d}{Z_0})} \qquad (1)$$

### 3.4 Modeling Approach

The modeling approach used in this study quantifies a below-ground leak rate in three steps:

1. Make above-ground downwind measurements of $CH_4$ and meteorological data.
2. Use the above-ground measurements in a backward Lagrangian stochastic (bLs) atmospheric dispersion model to estimate the surface emission rate.
3. Use the surface-emission rate to calculate the below-ground leak rate in the inverse ESCAPE model; henceforth referred to as the $ESCAPE^{-1}$ model (Section 3.4.2).

#### *3.4.1 The backward Lagrangian stochastic model (bLs)*

The bLs model models the path of particles using concentration measurement from the receptor location to the source of particles (Flesch et al., 2004). As mentioned in section 2.2.2, a below-ground leak presents as an area source of $CH_4$ emission; therefore, the bLs model is used to infer surface $CH_4$ flux from the source. Since concentration measurements in this study were sampled using a line-averaging sensor, this will be the basis for inferring the surface emission flux. In a

line-averaging sensor, concentration measurement ($C_L$, in ppm-m; Equation 2) is the average of P point concentrations that are equidistant along the line of sight of the laser path (Flesch et al., 2004).

$$(C_L|Q)_{sim} = \frac{1}{P}\sum_{J=1}^{p}\left(\frac{1}{N}\sum\left|\frac{2}{w_0}\right|\right) \qquad (2)$$

Where $N$ is the number of particles released from the measurement point downwind, and $w_0$ is the impact of the backward trajectories from the sensor to the source. The surface flux, $Q_{bLs}$, is derived using equation 3.

$$Q_{bLs} = \frac{C_L - C_b}{(C_L|Q)_{sim}} \qquad (3)$$

Where $C_b$ is the background concentration of $CH_4$ measured upwind of the source (Flesch et al., 2004).

The surface emission rates ($Q_s$, g $m^2$ $s^{-1}$) were calculated using WindTrax's bLs model (WindTrax Version 2.0; (Crenna, 2006)). WindTrax is suitable for near-field measurements i.e., within 1 km of the source, and is accurate when measurements are taken on a flat surface and within an area free of obstructions (Crenna, 2006; Flesch et al., 2004;2005). The bLs model is used because, 1 It is suitable for estimating emissions from an area source using above-ground downwind measurements, 2 It can be applied to below-ground pipelines installed in rural environments, and beneath a flat terrain in an area free of obstructions (Crenna, 2006).

Input to the bLs model included 10-minute average $CH_4$ mixing ratios, wind speed, and wind direction. 10-minute $CH_4$ mixing ratios, wind speed, and wind direction averages were calculated to represent the mean atmospheric state during an experiment (Crenna, 2006). Measurements were classified into 4 different PGSC (Pasquill-Gifford stability classes A, B, C, D) based on the wind speed and daytime solar insolation (Pasquill, 1961; Table A1.2). PGSC A, B, C, and D correspond

to extremely unstable, moderately unstable, slightly unstable, and neutral atmospheric conditions, respectively.

In the bLs model, the input included setting the surface roughness length at 0.023 m to represent the short grass cover on the testbed (Table A1.3) and setting the background $CH_4$ mixing ratio, measured upwind of the controlled emission. Other parameters required to run the simulation include the Monin-Obukhov length ($L$, m; defined in Table A1.4), and the friction velocity ($u^*$, m $s^{-1}$). WindTrax calculated these parameters internally based on the wind speed, and PG stability classes.

The point on the surface that is located directly above the leak will record the highest concentrations of $CH_4$; this is referred to as the 'focus' (Riddick et al., 2021). At 0.5 m distance increments from the focus, a leak that is greater than or equal to 0.2 kg $h^{-1}$ forms an emission radius of up to 4.5 m on the surface. The surface $CH_4$ concentrations decrease exponentially from the focus (Cho et al., 2020; Riddick et al., 2019). During experiments, surface $CH_4$ measurements taken using a Bascom Turner gas rover migrated up to a maximum of 4.5 m from the 'focus'. Therefore, for the conditions tested in this study (0.2, 0.4, and 0.8 kg $h^{-1}$ controlled leak rates, dry soil, grass surface cover, and no underground preferential pathways), a homogenous area source of emission (radius = 4.5 m) on the surface was used.

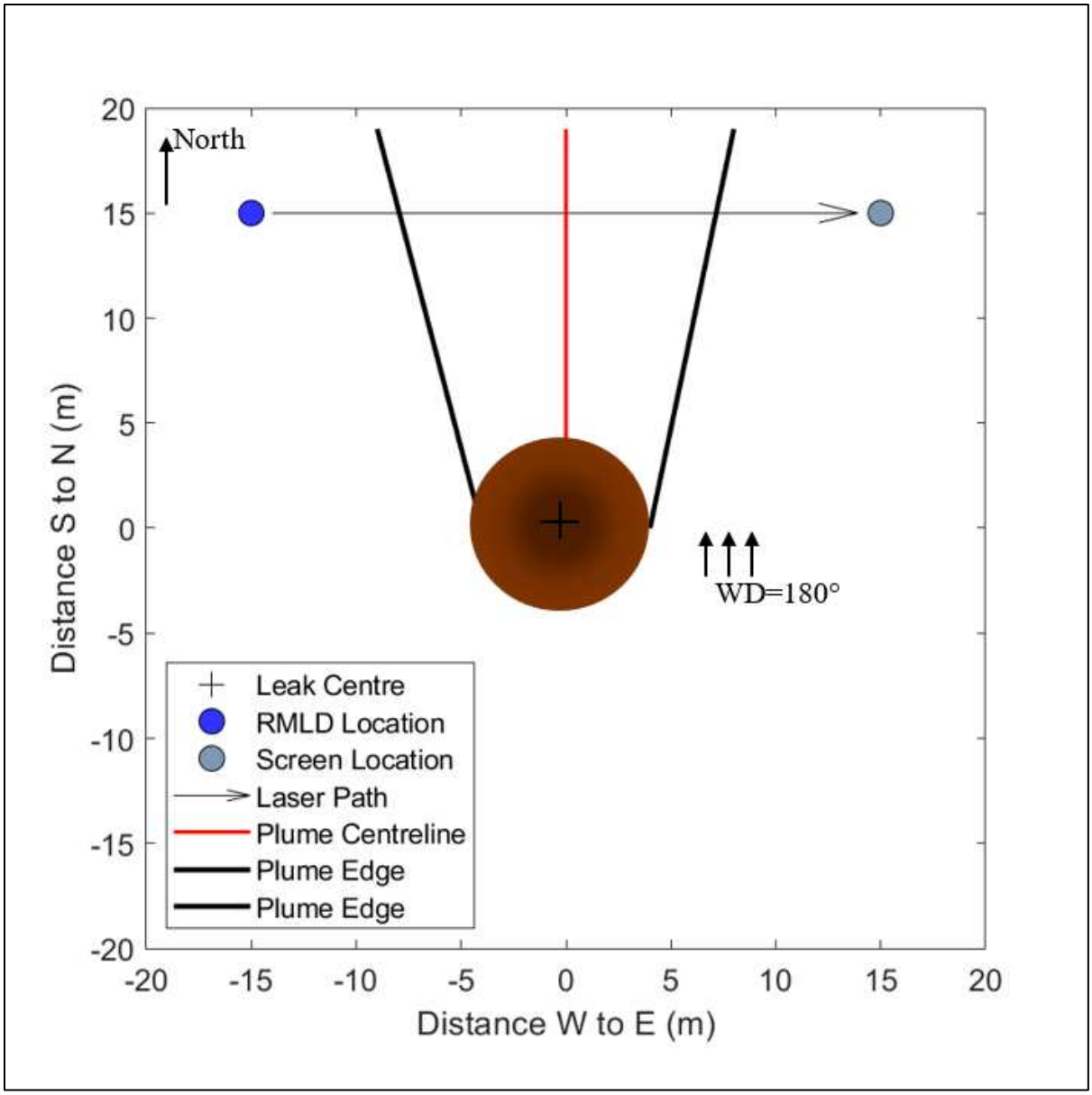


*Figure 4. Top view schematic representation of the surface expression of a leak, location of the RMLD, and the screen during an experiment when the wind direction is 180° (from the south). The emission radius is set at 4.5 m to represent the distance of surface gas migration from the leak center. The plume centerline has the highest concentrations of $CH_4$, and the concentrations decrease towards the plume edge. The above-ground setup is as follows, i.) The reflective screen was located directly opposite the RMLD in all experiments, ii.) The combination was positioned 15 m downwind of the leak, and iii.) The path length was set perpendicular to the wind direction.*

### *3.4.2 The ESCAPE$^{-1}$ model.*

The ESCAPE model was developed by Riddick et al., 2021 to estimate surface $CH_4$ concentrations. In Equation 4, gas flow to the atmosphere, $Q_x$, is a function of the gas mixing ratio from the leak ($X_l$), the gas mixing ratio in the atmosphere ($X_{at}$), resistance to gas flow in the soil ($R_s$), and resistance to gas flow in the atmosphere ($R_{at}$).

$$Q_x = \frac{X_l - X_{at}}{R_{at} + R_s} \quad (4)$$

For gas leaks in gathering and distribution systems, the flow in the soil is limited by diffusion assuming that advection affects only a small section near the leak (Mitton, 2018). Here, the rate of diffusion is a function of the concentration gradient and the diffusion coefficient. Therefore, the diffusive flux in the soil ($f_d$: Equation 5) is obtained through Fick's law and is considered a product of the concentration gradient ( $\nabla C$, g m$^{-4}$) and diffusion coefficient ($D_p$, m$^2$ s$^{-1}$)

$$f_d = -D_p \nabla \mathrm{C} \quad (5)$$

To model gas flow in the sub-surface (Figure 5), ESCAPE assumes that:

1. The soil properties affecting diffusion are uniform in the region.
2. Gas flow is inversely proportional to the resistance of flow.
3. Resistance of gas flow is inversely proportional to the distance gas will travel to the surface.
4. Surface emission at a perpendicular distance from the leak can be scaled to the actual size of the leak.
5. Gas flow is in a steady state, and only vents to the atmosphere i.e., it does not vent into any nearby structures.

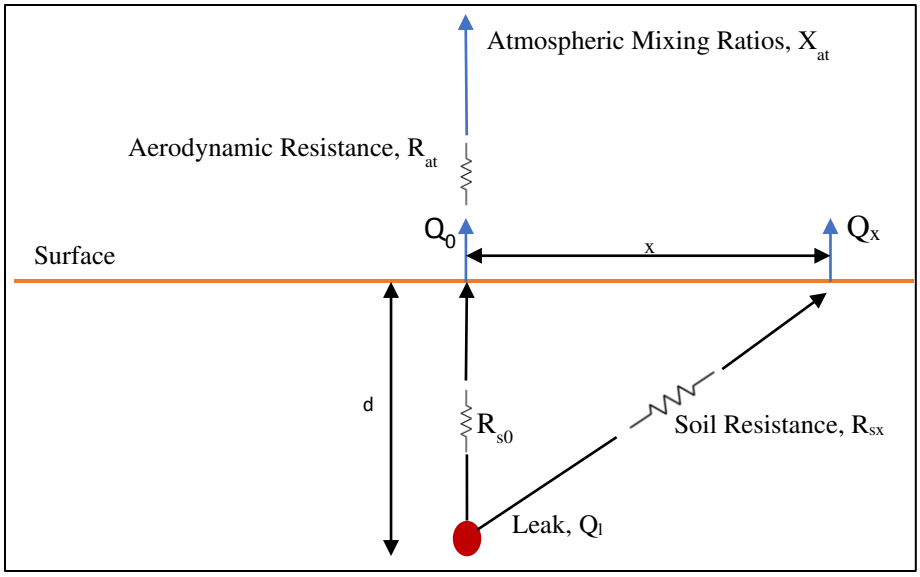


*Figure 5. Below-ground to above-ground gas flow showing the assumptions made by the ESCAPE model (Riddick et al., 2021)*

Using the assumptions above, the ESCAPE model defines the surface $CH_4$ flux at a distance x from the focus ($F_x$, g $m^{-2}$ $s^{-1}$: Equation 6).

$$F_x = \left(\frac{Q_T}{A_x}\right)\left(\frac{Q_x}{\sum_{x=0}^{\infty} Q_x}\right) \quad (6)$$

The surface $CH_4$ flux ($F_x$) is defined as a function of the total emission rate ($Q_T$), area of the surface expression of the leak ($A_x$, $m^2$: Equation 8), emission at a distance x ($Q_x$, g $s^{-1}$: Equation 7), and the sum of emission rates at distances from the focus ($\sum Q_x$, g $s^{-1}$).

$$Q_x = \frac{V}{\sqrt{X^2+d^2}} \quad (7)$$

$$A_x = \pi\left(\left(x+\frac{x}{2}\right)^2 - \left(x-\frac{x}{2}\right)^2\right) \quad (8)$$

The resistance to gas flow in the atmosphere (Equation 9) is a sum of aerodynamic resistance ($R_a$, m $s^{-1}$: Equation 11), and boundary layer resistance ($R_b$, m $s^{-1}$: Equation 10).

$$R_{at} = R_a + R_b \quad (9)$$

The boundary layer resistance describes the flow of gas through the vegetation on the surface (Equation 10). It is a product of the boundary layer Stanton number ($B$=5) and the friction velocity ($u^*$, m $s^{-1}$).

$$R_b = (Bu^*)^{-1} \quad (10)$$

The aerodynamic resistance (Equation 11) is derived as a function of the zero-plane displacement length ($z_d$, m), the roughness length ($z_0$, m), the Monin-Obukhov length ($L$, m), and the product of Von Karman constant ($k$ = 0.41) and the wind speed ($u$, m $s^{-1}$). The Von Karman constant

$$R_a = \frac{\left[\ln\left(\frac{z-z_d}{z_0}\right) - \psi_m\left(\frac{z-z_d}{L}\right)\right]^2}{k^2 u} \qquad (11)$$

In Equation 11 above, a stability correction factor ($\psi_m$) is obtained for both the stable and the unstable conditions (Equations 12 and 13).

$$\psi_m\left(\frac{z}{L}\right) = -\frac{5z}{L} \qquad (12)$$

$$\psi_m\left(\frac{z}{L}\right) = 2\ln\left(\frac{1+X}{2}\right) + \ln\left(\frac{1+X^2}{2}\right) - 2tan^{-1}(X) + \frac{\pi}{2} \qquad (13)$$

Where, $X = (1 - 16(\frac{z}{L}))^{1/4}$

Applying Ohm's law resistance analogy, the ESCAPE model estimates the surface $CH_4$ concentration ($X_x$, ppm: Equation 14) using $F_x$ (Equation 6), a background concentration ($X_a$) of 1.9 ppm, and atmospheric resistance $R_{at}$ (Equation 9).

$$X_x = F_x R_{at} + X_a \qquad (14)$$

To estimate the below-ground leak rate in the ESCAPE[-1] model, the model assumes that the surface emission is the sum of the product of surface fluxes ($Q_X$: Equation 2.4), and the area of surface expression ($A_X$: Equation 2.5) of the leak ($\sum Q_x A_x$, g $m^2$ $s^{-1}$). Here, the model assumes that at the surface, the leak presents as an area source (concentric-like gas migration) with the highest concentration of gas at the point that is directly above the leak, known as the leak center in this study.

The emission ($Q_x$, g $s^{-1}$) is derived at perpendicular distances from the leak (Figure 5) while the area of the surface expression ($A_x$: $m^2$) of the leak at 0.5 m distances from the focus is derived as a function of the emission radius (Equation 8).

In equation 7, $V$ is considered as the sum of advective flux, ($F_{Dx}$, Equation 15), and the diffusive flux ($F_d$: Table A1.1). The data used in Darcy's and Fick's law can be found in Table A1.1.

$$F_{Dx} = -\frac{k k_r \rho}{\mu} (\nabla P - \rho g) \quad (15)$$

Using the surface concentrations at each distance from the focal point, the model estimates individual flow rates from the leak point to each distance on the surface ($Q_x$, g $s^{-1}$).

The below-ground leak rate ($Q_l$, g $s^{-1}$: Equation 16) is derived as a function of an area correction factor ($A_f$= 0.044 $m^2$), the emission rates derived by the bLs model ($Q_S$, g $s^{-1}$), and the total surface flux ($\sum Q_x A_x$, g $m^2$ $s^{-1}$). The area correction factor accounts for the radial presentation of the leak.

$$Q_l = \frac{A_f * Q_S}{\sum_{x=0}^{\infty} Q_x A_x} \quad (16)$$

### 3.5 Uncertainty analysis

The causes of uncertainty in the modeling approach are the above-ground $CH_4$ measurements, the meteorological measurements (wind speed and wind direction), the surface expression of a leak, and the classification of atmospheric stability. Above-ground $CH_4$ measurements and meteorological data from the 0.4 kg $h^{-1}$ controlled release rate were used to evaluate the uncertainty in the modeling approach. The uncertainties were determined through a sensitivity analysis of the modeling approach in 3 different PG stability classes (A, B, and C). PGSC D was not used in the sensitivity analysis as it had too few data points (6 points) to be used for comparison.

The major steps in the sensitivity analysis are:

1. To derive surface emission using WindTrax's bLs model.
2. To derive below-ground leak rates using the $ESCAPE^{-1}$ model.
3. To calculate the standard deviation (this is used to present uncertainty in each case) using the estimated leak rate in PG stability classes A, B, and C.

The standard deviation was calculated using equation 17, where ELR represents the estimated leak rate in kg $h^{-1}$, 0.4 is the known leak rate in kg $h^{-1}$, and n is the number of estimated leak rates in each stability class. The calculated uncertainty from PG stability class B is used to present the uncertainty in the estimated leak rate (0.4kg $h^{-1}$ ± standard deviation in kg $h^{-1}$).

$$std = \sqrt{\frac{\sum_i^n (ELR_i - 0.4)^2}{(n-1)}} \qquad (17)$$

Individual uncertainties were propagated to the estimated leak rate using equation 18.

$$\sigma_{ELR}^2 = (\frac{\delta(ELR)}{\delta(M)})^2\sigma_M^2 + (\frac{\delta(ELR)}{\delta(WS)})^2\sigma_{WS}^2 + (\frac{\delta(ELR)}{\delta(WD)})^2\sigma_{WD}^2 + (\frac{\delta(ELR)}{\delta(A)})^2\sigma_A^2 + (\frac{\delta(ELR)}{\delta(P)})^2\sigma_P^2 \qquad (18)$$

Equation 18 is a sum of the product of the derivatives and the variance from each source of uncertainty. Where each of the derivatives in the equation represents the derivative of ELR (estimated leak rate) with respect to: *M* the $CH_4$ mixing ratio in ppm-m, *WS* the wind speed in m $s^{-1}$, *WD* the wind direction, *A* the area of the source of emission, and *P* the classification of atmospheric stability.

# 4 RESULTS

Above-ground $CH_4$ mixing ratio measurements were taken from the rural testbed at METEC between 27 September to 3rd December 2021 and controlled release rates were set at 0.2, 0.4, and 0.8 kg $h^{-1}$ (Table 1). During the experiments, wind speeds were generally low (< 3 m $s^{-1}$) and the atmosphere was generally unstable (Table 1). Average mixing ratios were in the order of 70 to 110 ppm m. Generally, the orientation of the RMLD relative to the plume edge and the plume centerline affected the estimated leak rate, therefore data quality control was done to account for this impact.

## 4.1 Data quality control

### *4.1.1 Wind direction*

Ideally, the RMLD laser's path should cut across the centerline of an above-ground gas plume (Figure 4; (Heath, 2009)). The gas concentration within the plume is heterogeneous and the plume centerline has the highest concentration i.e., from this line, the concentration of gas reduces outwards (Figure A5; Stull, 2015). The bLs model can accurately calculate emissions when the laser is perpendicular to the plume centerline (Flesch et al., 2005; Flesch & Wilson, 2005) (Figure 4). This study suggests that rapid changes in wind direction (by 26º) in a 10-minute time interval may align the RMLD's laser along the plume centerline, i.e., along the region of high $CH_4$ concentrations (Stull, 2015), causing the bLs model to overestimate the surface emission and result in a subsequent overestimation of below-ground leak rates.

In addition, a shift in the plume centerline can mean that the sensor is measuring at the plume edge (Figure 4; Figure A5). At the plume edge, gas molecules are defined by extreme and less predictable paths (Flesch et al., 2005;2004; Flesch & Wilson, 2005; Stull, 2015). Methane measurements from the plume edge are an average of low concentrations (Figure A5), therefore,

these $CH_4$ measurements underestimate the below-ground leak rate. As a result of these, data were removed when the change in wind direction was ≥ 26° over the 10-minute averaging period.

There was a total of 226 10-minute averaged data points (merged $CH_4$ measurements, and meteorological data). These data points were classified into PG stability classes A, B, C, and D. Each of the points derived a surface emission rate in the bLs model, and a sequential leak rate in the ESCAPE$^{-1}$ model (Figure 6). After filtering for wind direction, a total of 173 points remained.

#### *4.1.2 Wind speed*

Accurate estimation of the emission rate in the bLs model depends on accurate measurement of concentration (Flesch & Wilson, 2005). At low wind speeds, gas may not travel from the source to the RMLD detector, resulting in the violation of assumptions of constant air flow made by the bLs model (Crenna, 2006; Flesch & Wilson, 2005). Additionally, the ESCAPE$^{-1}$ model underestimates the leak rate by 54% when the wind speed is < 2 m s$^{-1}$. Following the experimental methods of Flesch et al. (2004 & 2005), data were removed when the average wind speed during the experiment was less than 2 m s$^{-1}$. After filtering for wind speed, a total of 113 data points remained (Figure 6).

### 4.2 Uncertainty analysis

The accuracy to which the RMLD could measure the $CH_4$ mixing ratio in the air caused the largest uncertainty in leak rate, as calculated by the ESCAPE$^{-1}$ model (±28%). The uncertainties from the wind speed and the wind direction are ±18% and ±8%, respectively. The surface expression of a leak presented an uncertainty of ±38%, whereas uncertainty in assigning PGSC using the method described in Section A1.2 resulted in an uncertainty of ±30%. Assuming that the individual uncertainties are inherent, these individual uncertainties were propagated to the estimated leak rate to obtain the overall uncertainty. The overall uncertainty in the modeling approach is estimated at ±25% (Table A3.6).

### 4.3 Methane mixing ratios, surface emissions, and calculated leak rates

10-minute averaged $CH_4$ mixing ratios observed during the 113 experiments ranged from 193 ppm m to 28 ppm m. During the 0.2 kg $h^{-1}$ controlled leak experiment, the smallest, largest, and average measured $CH_4$ mixing ratios were 56, 84, and 71 ppm-m, respectively (Figure 6a). During the 0.4 kg $h^{-1}$ controlled leak, the smallest, largest, and average measured $CH_4$ mixing ratios are 28, 193, and 82 ppm-m, respectively. During the 0.8 kg $h^{-1}$ controlled leak, the smallest, largest, and average measured $CH_4$ mixing ratios are 50, 238, and 122 ppm-m, respectively.

Using the 10-minute averaged $CH_4$ mixing ratio in the bLs model, individual surface emissions ranged from 0.010 to 0.043 g $m^{-2}$ $s^{-1}$. For the 0.2 kg $h^{-1}$ controlled leak experiment, the smallest, largest, and average derived surface emission rates are 0.010, 0.013, and 0.010 g $m^{-2}$ $s^{-1}$, respectively (Figure 6b). For the 0.4 kg $h^{-1}$ controlled leak experiment, the smallest, largest, and average derived surface emissions are 0.004, 0.025, and 0.013 g $m^{-2}$ $s^{-1}$, respectively. For the 0.8 kg $h^{-1}$ controlled leak experiment, the smallest, largest, and average derived surface emissions are 0.013, 0.043, and 0.024 g $m^{-2}$ $s^{-1}$, respectively.

Using the surface emission rates as input to the ESCAPE$^{-1}$ model, individually calculated leak rates ranged from 0.03 to 1.31 kg $h^{-1}$. For the 0.2 kg $h^{-1}$ experiment, the smallest and largest estimated leak rates are 0.03 (-85%) and 0.40 (+100%) kg $h^{-1}$, respectively (Figure 6c). For the 0.4 kg $h^{-1}$ experiment, the smallest and largest estimated leak rates are 0.13 (-68%) and 0.75 (+88%) kg $h^{-1}$, respectively. For the 0.8 kg $h^{-1}$ experiment, the smallest and largest estimated leak rates are 0.40 (-50%) and 1.31 (+64%) kg $h^{-1}$, respectively.

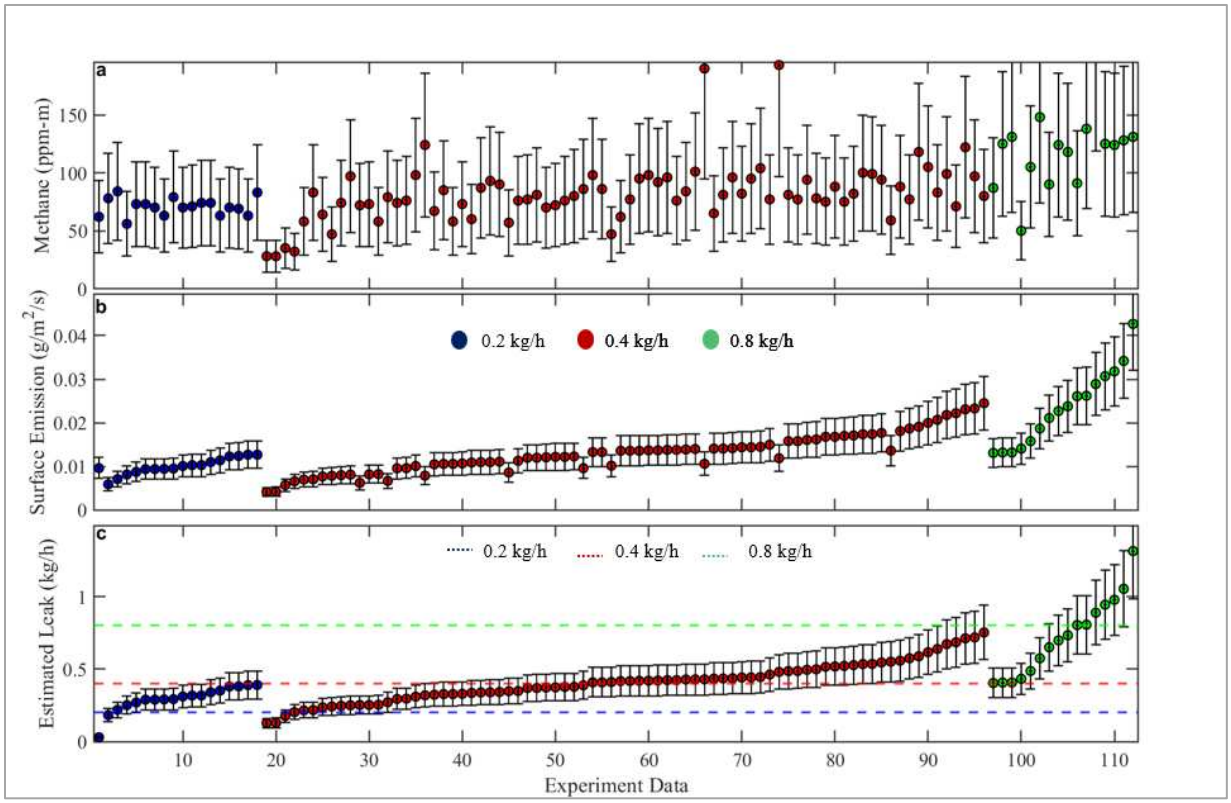


*Figure 6. Plot a is the 10-minute averaged $CH_4$ mixing ratios from measurements sampled by the RMLD, plot b is the surface emission as derived by the bLs model using $CH_4$ mixing ratios, and plot c is the estimated leak rate as derived by the ESCAPE$^{-1}$ model using the surface-emission. Error bars in plot a represent the uncertainty (±50%) due to the $CH_4$ mixing ratios. Error bars in plots b and c represent the uncertainty (±25%) in the modeling approach.*

Results of a Pearson's correlation test show that relative humidity and temperature do not correlate with the estimated leak rate ($R^2$ = 0.015 and 0.104, respectively; Section A7), as such, the discussion is not focused on the two variables. Both wind speed and atmospheric stability significantly affect the estimated leak rate (p-value less than 0.05), therefore, the results and discussion are focused on these impacts.

### 4.4 Effect of time averaging

When all individual leak rates based on 10-minute averaged data (Figure 6c) are averaged for each known leak rate, average below-ground leak rates are estimated at 0.31 (95% CI: 0.30, 0.32), 0.41 (95% CI: 0.38, 0.44), and 0.75 (95% CI: 0.69, 0.81) kg $CH_4$ $h^{-1}$ for the 0.2, 0.4, and 0.8 kg $CH_4$ $h^{-1}$ controlled leaks, respectively (Figure 7). Estimated leak rates in Figure 7 were averaged over 5, 3, and 4 hours for the 0.2, 0.4, and 0.8 kg $CH_4$ $h^{-1}$ controlled leaks, respectively, as compared to the 10-minute averages in Figure 6. Results suggest that the ESCAPE$^{-1}$ overestimates small leaks (0.2 kg $CH_4$ $h^{-1}$) by an average of 0.11kg $h^{-1}$ and underestimates large leaks (0.8 kg $CH_4$ $h^{-1}$) by an average of 0.05 kg $h^{-1}$. The linear regression of the average calculated leak rates against the known leak rate shows good agreement (m = 0.75; $R^2$ = 0.99, p-value = 0.07).

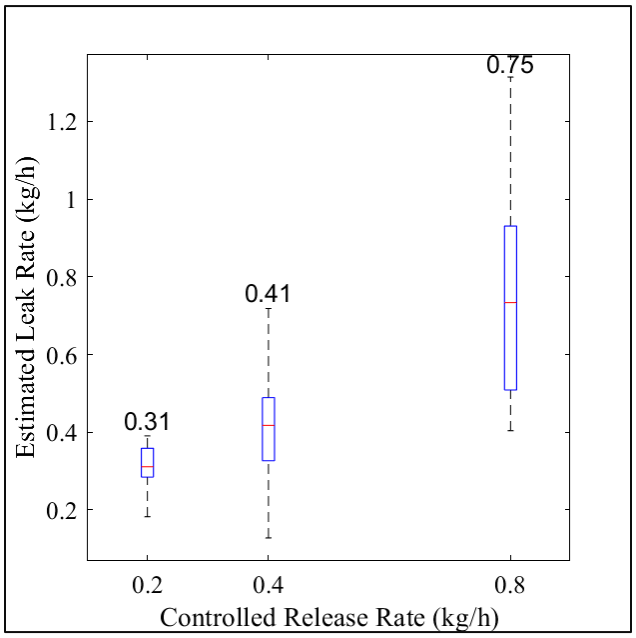


*Figure 7. Estimated leak rates from 0.2, 0.4, and 0.8 kg $CH_4$ $h^{-1}$ controlled release rates, respectively. This box plot was generated using the 10-minute averaged data points of the estimated leak rate that remained in each category of controlled release rate after data filtering. The numbers inside the plot represent the mean estimated leak rate in each controlled release rate. The number of data points used are 17, 77, and 15 points in the 0.2, 0.4, and 0.8 kg $CH_4$ $h^{-1}$ controlled release rates, respectively. The red line inside the box represents the median value, the boxes represent the 25$^{th}$, and the 75$^{th}$ percentiles, and the dotted black lines (the whiskers) represent ±1.5 times the interquartile range.*

### 4.5 Effect of wind speed

Figure 8 shows the estimated leak rate (ELR) plotted versus wind speed from the 0.4 kg $CH_4$ $h^{-1}$ controlled leak. The ELRs in Figure 8 are binned at 0.1 m $s^{-1}$ wind speed increment. The error bars represent the Root Mean Square Error (RMSE) of the ELR from the known leak rate (KLR). A Pearson's correlation test between the deviation of KLR and average wind speed shows that wind speed has a statistically significant impact on the deviation of the estimated leak rate from the known leak rate ($m = 0.23$, $R^2 = 0.47$, p-value $= 2.88 \times 10^{-9}$). Here, the estimated leak rate is more accurate in lower wind speeds (Figure 8). When the wind speed is between 2 and 3 m $s^{-1}$, the estimated leak rate deviates by an average of 0.1 kg $h^{-1}$ from the known leak rate with an RMSE of 0.12. As the wind speed increases to 4.5 m $s^{-1}$, the estimated leak rate deviates by an average of 0.2 kg $h^{-1}$ from the known leak rate with an RMSE of 0.04.

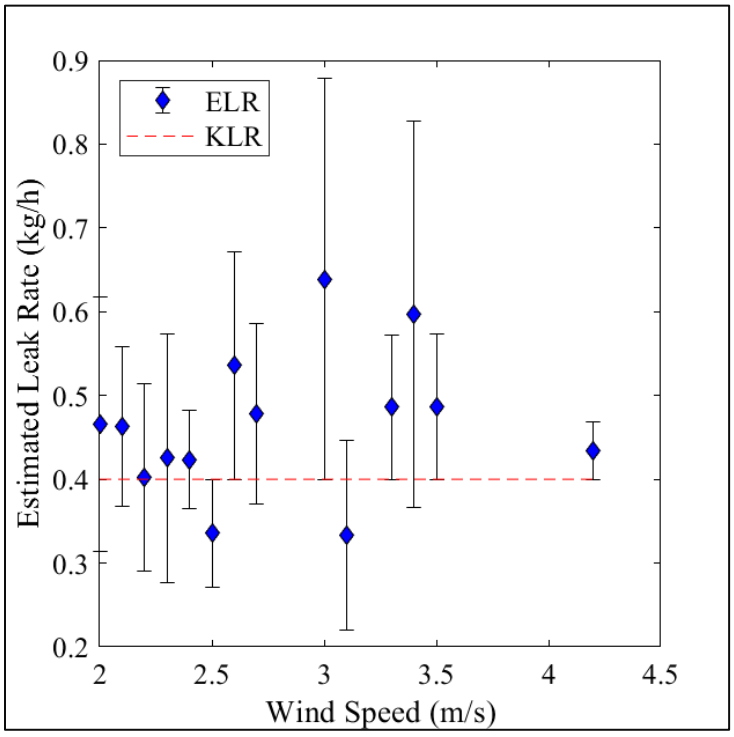


*Figure 8. Average estimated leak rate in wind speed from 2 to 4.5m $s^{-1}$. Estimated leak rates from the 0.4 kg $CH_4$ $h^{-1}$ controlled leak rate was binned by 0.1m $s^{-1}$ wind speed increments and used to generate this plot. The error bars represent the RMSE of each data point from the known leak rate. The red line is the known leak rate (KLR), and the blue points are the estimated leak rates (ELR). The model underestimates the leak rate when the wind speed is below 2m $s^{-1}$.*

### 4.6 Effect of atmospheric stability

Figure 9 shows a box plot of the difference between the Estimated leak rate, $Q_E$, and the known leak rate, $Q_K$ in PGSC B, and C. This Plot was generated using 10-minute averaged data points after data filtering (Section 4.1). The difference between the known and estimated leak rates from PGSC A is not shown in Figure 9 because this stability class was filtered out during the data quality control in section 4.1. PGSC A belongs to measurements when the wind speed is less than 2 m $s^{-1}$ and during extremely unstable conditions. Results show that the ESCAPE$^{-1}$ model estimates the below-ground leak rate with an average bias of 12%, and -5% in PGSC B, and C, respectively (Figure 9). This shows that the modeling approach works best during moderately unstable (PGSC B), and slightly unstable (PGSC C) atmospheric conditions. PG stability class D is not included in the comparison because this category had 6 data points and represents neutral conditions of the atmosphere.

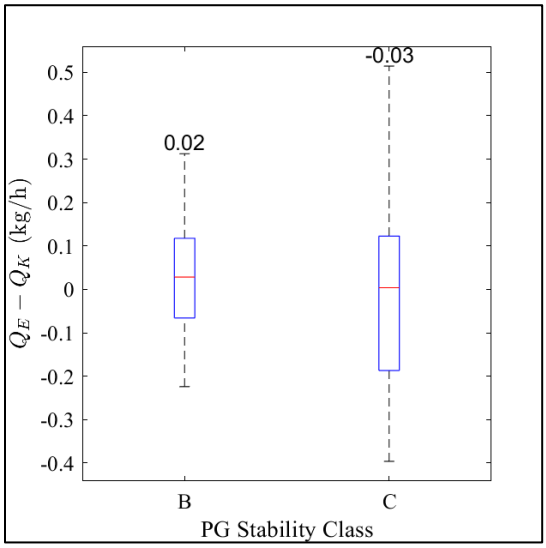


*Figure 9. Difference between the estimated and the controlled release rate ($Q_E$-$Q_K$) in PGSC B, and C. The red lines inside the boxes represent the median value* of the difference between the estimated and the known leak rate in each stability class*, while the boxes represent the 25$^{th}$ and the 75$^{th}$ percentiles. The dotted black lines (the whiskers) represent ±1.5 times the interquartile range. The numbers inside the plots represent the average difference in each stability class. The number of data points used is 73, and 27 in PGSC B, and C, respectively. PGSC A was not used in the plot because it has few data points (6) after filtering for WS, and change in WD. Also, PGSC D was not used in the plot because it has 6 data points and represents the neutral conditions of the atmosphere.*

# 5 DISCUSSION

## 5.1 Instrumentation: The Remote Methane Leak Detector

The work presented here used above-ground, line-averaged $CH_4$ mixing ratios measured by a lower-cost, lower-precision TDLAS $CH_4$ detector. Results show that when measuring downwind of a below-ground leak point, if the sensor's laser path cut across the plume edge, then the reported mixing ratio is likely to be an underestimate of the below-ground leak rate because it will have only measured the edge of the plume, i.e., a region of lower concentrations of $CH_4$. This can happen when the wind direction varies more than 25° over the 10-minute measurement period or during extremely unstable, low-wind atmospheric conditions when the plume can loft over the laser's path, i.e., PGSC A. Therefore, this study recommends that the below-ground leak rate quantification approach presented here should only be used if the laser path is perpendicular and at the same height as the plume centerline (Figure 4).

## 5.2 Performance of the ESCAPE$^{-1}$ model.

Using 10-minute averaged $CH_4$ mixing/meteorological data and filtering out low wind/PGSC A events, the ESCAPE$^{-1}$ model estimates small distribution leaks (0.2 kg $CH_4$ $h^{-1}$) with an average bias of -85%/+100%, and medium distribution leaks with an average bias of (0.8 kg $CH_4$ $h^{-1}$) to -50%/+64% (Figure 6c). Large distribution leaks, > 1 kg $CH_4$ $h^{-1}$ (Weller et al., 2018; Hendrick et al., 2016; Lamb et al., 2015) were not tested due to concerns about damaging the test bed. When averaged over a longer period (more than 3 hours of data), the average calculated leak rate was an overestimate of +55% for the small (0.2 kg $CH_4$ $h^{-1}$) leak and an underestimate of -6 % for a medium distribution leak (0.8 kg $CH_4$ $h^{-1}$).

These data suggest that 10-minute averaged data used as input to the ESCAPE$^{-1}$ approach could be used to distinguish between small and medium distribution leaks, but it can more accurately

quantify larger leaks than smaller leaks and accuracy improves if the measurement time is increased. This is likely caused by the size of the plume created by the emission, where larger leak rates result in a larger plume, and it is more probable that the instrument's laser path will be perpendicular and level with the plume centerline. The ESCAPE$^{-1}$ model works poorly during extremely unstable atmospheric conditions and in wind speeds less than 2 m s$^{-1}$. If used in these conditions, it will likely underestimate the below-ground leak rate and the total emissions from a pipeline.

### 5.3 Effect of wind speed

Results also suggest that as the wind speed increases from 2 to 5 m s$^{-1}$, both the accuracy and precision of the leak rate calculated by the ESCAPE$^{-1}$ model decrease. Wind, and particularly its turbulence, is a significant agent in dispersing any gas released into the atmosphere (Lines et al., 1997). Therefore, as the wind speed increases, gas disperses less as it travels from the source to the atmosphere, resulting in a collimated plume that could be undetected by the instrument's laser. Observations at the METEC site suggest that wind speeds are often less than 2 m s$^{-1}$ (Section A6) and studies have shown that most atmospheric dispersion models, including the bLs model, are inaccurate in estimating emissions during low wind speeds (Bai et al., 2022; Deaves & Lines, 1998; T. Flesch et al., 2005; Lines et al., 1997). In the real world, waiting for ideal wind conditions to estimate emissions may conflict with the operator's schedule and measurements need to be made regardless of meteorology.

### 5.4 Effect of Atmospheric Stability

In addition to wind speed, results also indicate that the ESCAPE$^{-1}$ model is better at estimating the below-ground leak rate as the atmosphere becomes more unstable, i.e., PGSC B is better than PGSC C. As mentioned above, PGSC A data should not be used as it is likely that the plume will not reach the detector in low wind and an extremely unstable atmosphere. Results of this study

suggest PGSC B conditions result in better leak size estimates as the plume will be more vertically mixed with a less defined plume center that could be undetected by the laser. This suggests something of a measurement pay-off between atmospheric conditions that transport the gas from the source to the detector, but also with enough vertical mixing to make the plume more homogenous.

### 5.5 Suggested improvements to the modeling approach

The main sources of uncertainty in the modeling approach were the measurement of the $CH_4$ mixing ratios using a line averaging TDLAS detector and atmospheric stability classification. A line-averaging TDLAS sensor was used instead of a point sensor, i.e., the Gas Rover, for above-ground $CH_4$ measurements because it provides flexibility in accessing difficult-to-access leak locations and would measure across the plume, i.e., more likely to detect the plume. However, the accuracy in the TDLAS instrument depends on how well the gas has dispersed allowing the laser to cross the plume centerline. This study suggests that the 'better measurement condition' resulting in more accurate quantification using the ESCAPE$^{-1}$ approach is something of a pay-off between high enough wind to move the gas, but not too high that the plume becomes collimated and more easily undetected.

Atmospheric stability can be classified in many ways, including Pasquill Gifford's classification (Pasquill, 1961) or using Monin-Obukhov length (Breedt et al., 2018; Flesch et al., 2004). Here, a relatively low-tech approach of estimating the PGSC using wind speed and isolation was used as it is unlikely that operators would have access to instruments that could quantify the Monin-Obukhov length. As the uncertainty analysis has shown, the uncertainty associated with assigning PGSC is ±30% but this could be reduced by using a sonic anemometer, where the Monin-Obukhov length can be directly calculated, or by measuring wind speed and different heights and inferring

the Monin-Obukhov length from the change in wind concerning height above the ground (Breedt et al., 2018).

### 5.6 Measuring in more complex environments

The approach presented here was tested in a rural testbed comprising a grass surface with no sub-surface infrastructure, this only simulates a pipeline passing through undisturbed homogeneous soil. For gathering and transmission lines this may be reflective of the situation, but unlikely to simulate what is happening in the distribution network. All the measurements were taken on flat terrain with a vegetation surface cover (surface roughness = 2.3 cm for short grass: Table A1.3), and minimal obstruction such as nearby buildings (Figure A2). Here the study suggests that the ESCAPE$^{-1}$ model may not work to estimate pipeline leaks in complex aerodynamic environments such as an urban landscape. To address this, this study suggests testing the approach in more complex aerodynamic environments, where measurements are taken in an area with obstructions such as tall buildings, and above a less permeable surface cover such as asphalt. This will create a clear understanding of surface and above-ground gas flow in less permeable surface cover and possibly improve gas leak quantification in these complex geometries.

# 6 CONCLUSION AND RECOMMENDATIONS

This study investigated the environmental conditions in which lower-cost, industry-standard $CH_4$ detectors could be used to quantify leak rates from subsurface NG pipeline leaks installed in rural environments. Here, this study shows that averaged $CH_4$ concentration data measured using a $CH_4$ detector can be used to calculate leak rates between 0.2 and 0.8 kg $CH_4$ $h^{-1}$ in wind speeds above 2 m $s^{-1}$ when the pipeline is traveling through native soils. At a minimum this tool can be used to differentiate between a small (0.2 kg $CH_4$ $h^{-1}$) and a medium leak (0.8 kg $CH_4$ $h^{-1}$), this makes it possible to prioritize leak repair as current methods only use $CH_4$ detector data to generate a binary decision on whether the leak is a safety risk or not.

Recently, PHMSA proposed a revision to the regulations that implement the PIPES Act of 2020. The amendments would include modernizing old pipeline leak detection, leak grading, and leak repair rules by using technological methods to detect, grade, and repair leaks (PHMSA, 2023). Current methods such as flux chambers involve exposing the pipeline to accurately quantify the leak rate. Emission from a below-ground leak covers a large area on the surface and digging such an area to expose a pipeline takes time, yet operators cannot pinpoint the exact point in the pipeline that is leaking before exposing it. The modeling approach in this study provides a quick and efficient way of quantifying a below-ground leak while eliminating the need to expose a pipeline. Particularly, this may be of value when estimating leak size in the gathering pipeline network.

In line with modernizing traditional methods in pipeline safety, the modeling approach detailed in this study leverages industry-standard instruments to estimate the below-ground leak rate. The RMLD is a path-integrated instrument that can detect a leak from up to 30 m away, this means that it is suitable for leak locations that are ‘hard-to-reach’. Once an operator localizes a leak using the

RMLD, they can use above-ground measurements to estimate the leak rate in less than 30 minutes without digging up the pipeline.

Future work will investigate the possibility of improving the functionality of the modeling approach. This will involve investigating whether the approach can be applied to the distribution network with the potential of simulating two simultaneous leak points. Here, a larger testbed at METEC of 30 by 30 m (length by width) will be utilized to ensure that the distance of gas flow on the surface is accounted for. This is done by spacing the leak points with a distance greater than 9 m, this is because at the surface a single leak creates a diameter of 9 m. Further, aboveground measurements from two leak depths will be tested to assess the utility of the approach for NG pipelines buried at 0.6 and 1.8 m below the ground. Also, since the approach was tested in a controlled environment, future steps will involve testing the approach in an actual NG pipeline. The two individual models, the bLs model and the ESCAPE$^{-1}$ model, will be aggregated into a single software to improve efficiency of the approach for pipeline operators. Given that the accuracy of the approach depends on the orientation of the line-averaging sensor, this approach will be tested with measurements from a point sensor.

# 7 REFERENCES


*49 CFR Part 192 -- Transportation of Natural and Other Gas by Pipeline: Minimum Federal Safety Standards*. (n.d.). Retrieved September 4, 2023, from https://www.ecfr.gov/current/title-49/part-192

*101515-0-RMLD-MANUAL-REV-F.pdf*. (n.d.). Retrieved August 30, 2023, from https://heathus.com/assets/uploads/101515-0-RMLD-MANUAL-REV-F.pdf

*ANSI-GPTC-Z380-1-2022-Addendum-2-02_02_23.pdf*. (n.d.). Retrieved August 30, 2023, from https://www.aga.org/wp-content/uploads/2023/02/ANSI-GPTC-Z380-1-2022-Addendum-2-02_02_23.pdf

Bai, M., Loh, Z., Griffith, D. W. T., Turner, D., Eckard, R., Edis, R., Denmead, O. T., Bryant, G. W., Paton-Walsh, C., Tonini, M., McGinn, S. M., & Chen, D. (2022). Performance of open-path lasers and Fourier transform infrared spectroscopic systems in agriculture emissions research. *Atmospheric Measurement Techniques*, *15*(11), 3593–3610. https://doi.org/10.5194/amt-15-3593-2022

Baillie, J., Risk, D., Atherton, E., O'Connell, E., Fougère, C., Bourlon, E., & MacKay, K. (2019). Methane emissions from conventional and unconventional oil and gas production sites in southeastern Saskatchewan, Canada. *Environmental Research Communications*, *1*(1), 011003. https://doi.org/10.1088/2515-7620/ab01f2

Breedt, H. J., Craig, K. J., & Jothiprakasam, V. D. (2018). Monin-Obukhov similarity theory and its application to wind flow modelling over complex terrain. *Journal of Wind Engineering and Industrial Aerodynamics*, *182*, 308–321. https://doi.org/10.1016/j.jweia.2018.09.026

Cai, X., Peng, G., Guo, X., & Leclerc, M. Y. (2008). Evaluation of backward and forward Lagrangian footprint models in the surface layer. *Theoretical and Applied Climatology*, *93*(3–4), 207–223. https://doi.org/10.1007/s00704-007-0334-0

Chen, J., Dietrich, F., Maazallahi, H., Forstmaier, A., Winkler, D., Hofmann, M. E. G., Denier Van Der Gon, H., & Röckmann, T. (2020). Methane emissions from the Munich Oktoberfest. *Atmospheric Chemistry and Physics*, *20*(6), 3683–3696. https://doi.org/10.5194/acp-20-3683-2020

Cho, Y., Ulrich, B. A., Zimmerle, D. J., & Smits, K. M. (2020). Estimating natural gas emissions from underground pipelines using surface concentration measurements☆. *Environmental Pollution*, *267*, 115514. https://doi.org/10.1016/j.envpol.2020.115514

Crenna, B. (n.d.). *An introduction to WindTrax*.

Deaves, D. M., & Lines, I. G. (1998). The nature and frequency of low wind speed conditions. *Journal of Wind Engineering and Industrial Aerodynamics*, *73*(1), 1–29. https://doi.org/10.1016/S0167-6105(97)00278-X

*Delivery and storage of natural gas—U.S. Energy Information Administration (EIA)*. (n.d.). Retrieved September 5, 2023, from https://www.eia.gov/energyexplained/natural-gas/delivery-and-storage.php

EIA. (2022). *U.S. Energy Information Administration—EIA - Independent Statistics and Analysis*. https://www.eia.gov/todayinenergy/

EIA. (2023). *Natural gas and the environment—U.S. Energy Information Administration (EIA)*. https://www.eia.gov/energyexplained/natural-gas/natural-gas-and-the-environment.php

F, P. (1961). The estimation of the dispersion of windborne material. *Meteoro. Mag.*, *90*, 20–49.

Flesch, T. K., & Wilson, J. D. (2005). Estimating Tracer Emissions with a Backward Lagrangian Stochastic Technique. In J. L. Hatfield & J. M. Baker (Eds.), *Agronomy Monographs* (pp. 513–531). American Society of Agronomy, Crop Science Society of America, and Soil Science Society of America. https://doi.org/10.2134/agronmonogr47.c22

Flesch, T. K., Wilson, J. D., Harper, L. A., Crenna, B. P., & Sharpe, R. R. (2004). Deducing Ground-to-Air Emissions from Observed Trace Gas Concentrations: A Field Trial. *Journal of Applied Meteorology and Climatology*, *43*(3), 487–502. https://doi.org/10.1175/1520-0450(2004)043<0487:DGEFOT>2.0.CO;2

Flesch, T., Wilson, J., Harper, L., & Crenna, B. (2005). Estimating gas emissions from a farm with an inverse-dispersion technique. *Atmospheric Environment*, *39*(27), 4863–4874. https://doi.org/10.1016/j.atmosenv.2005.04.032

Gao, B., Mitton, M. K., Bell, C., Zimmerle, D., Deepagoda, T. K. K. C., Hecobian, A., & Smits, K. M. (2021). Study of methane migration in the shallow subsurface from a gas pipe leak. *Elementa: Science of the Anthropocene*, *9*(1), 00008. https://doi.org/10.1525/elementa.2021.00008

Gao, Z., Mauder, M., Desjardins, R. L., Flesch, T. K., & Van Haarlem, R. P. (2009). Assessment of the backward Lagrangian Stochastic dispersion technique for continuous measurements of CH4 emissions. *Agricultural and Forest Meteorology*, *149*(9), 1516–1523. https://doi.org/10.1016/j.agrformet.2009.04.004

Hadi, D. F. A. (n.d.). *Diagnosis of the Best Method for Wind Speed Extrapolation*. *4*.

Hendrick, M. F., Ackley, R., Sanaie-Movahed, B., Tang, X., & Phillips, N. G. (2016). Fugitive methane emissions from leak-prone natural gas distribution infrastructure in urban

environments. *Environmental Pollution*, *213*, 710–716. https://doi.org/10.1016/j.envpol.2016.01.094

Howard, T. (2015). University of Texas study underestimates national methane emissions at natural gas production sites due to instrument sensor failure. *Energy Science & Engineering*, *3*(5), 443–455. https://doi.org/10.1002/ese3.81

IPCC. (2013). Climate Change 2013: The Physical Science Basis. Contribution of Working Group I to the Fifth Assessment Report of IPCC the Intergovernmental Panel on Climate Change. In *Stocker, T. F.; Qin, D.; Plattner, G.-K.; Tignor, M. M. B.; Allen, S. K.; Boschung, J.; Nauels, A.; Xia, Y.; Bex, V.; Midgley, P. M. (eds.) (2014). Climate Change 2013: The Physical Science Basis. Contribution of Working Group I to the Fifth Assessment Report of IPCC the Intergovernmental Panel on Climate Change. Cambridge: Cambridge University Press 10.1017/CBO9781107415324 <http://dx.doi.org/10.1017/CBO9781107415324>*. Cambridge University Press. https://boris.unibe.ch/71452/

Jackson, R. B., Down, A., Phillips, N. G., Ackley, R. C., Cook, C. W., Plata, D. L., & Zhao, K. (2014). Natural Gas Pipeline Leaks Across Washington, DC. *Environmental Science & Technology*, *48*(3), 2051–2058. https://doi.org/10.1021/es404474x

Kang, M., Kanno, C. M., Reid, M. C., Zhang, X., Mauzerall, D. L., Celia, M. A., Chen, Y., & Onstott, T. C. (2014). Direct measurements of methane emissions from abandoned oil and gas wells in Pennsylvania. *Proceedings of the National Academy of Sciences*, *111*(51), 18173–18177. https://doi.org/10.1073/pnas.1408315111

Lamb, B. K., Cambaliza, M. O. L., Davis, K. J., Edburg, S. L., Ferrara, T. W., Floerchinger, C., Heimburger, A. M. F., Herndon, S., Lauvaux, T., Lavoie, T., Lyon, D. R., Miles, N., Prasad, K. R., Richardson, S., Roscioli, J. R., Salmon, O. E., Shepson, P. B., Stirm, B. H., &

Whetstone, J. (2016). Direct and Indirect Measurements and Modeling of Methane Emissions in Indianapolis, Indiana. *Environmental Science & Technology*, *50*(16), 8910–8917. https://doi.org/10.1021/acs.est.6b01198

Lamb, B. K., Edburg, S. L., Ferrara, T. W., Howard, T., Harrison, M. R., Kolb, C. E., Townsend-Small, A., Dyck, W., Possolo, A., & Whetstone, J. R. (2015). Direct Measurements Show Decreasing Methane Emissions from Natural Gas Local Distribution Systems in the United States. *Environmental Science & Technology*, *49*(8), 5161–5169. https://doi.org/10.1021/es505116p

Lines, I. G., Deaves, D. M., & Atkins, W. S. (1997). Practical modelling of gas dispersion in low wind speed conditions, for application in risk assessment. *Journal of Hazardous Materials*, *54*(3), 201–226. https://doi.org/10.1016/S0304-3894(96)01873-0

Lowry, D., Fisher, R. E., France, J. L., Coleman, M., Lanoisellé, M., Zazzeri, G., Nisbet, E. G., Shaw, J. T., Allen, G., Pitt, J., & Ward, R. S. (2020). Environmental baseline monitoring for shale gas development in the UK: Identification and geochemical characterisation of local source emissions of methane to atmosphere. *Science of The Total Environment*, *708*, 134600. https://doi.org/10.1016/j.scitotenv.2019.134600

Mitton, M. (n.d.). *Subsurface Methane Migration from Natural Gas Distribution Pipelines as Affected by Soil Heterogeneity: Field Scale Experimental and Numerical Study* [M.S., Colorado School of Mines]. Retrieved August 30, 2023, from https://www.proquest.com/docview/2129711130/abstract/4877DE588E184AE4PQ/1

Mohan, M. (1998). Analysis of various schemes for the estimation of atmospheric stability classification. *Atmospheric Environment*, *32*(21), 3775–3781. https://doi.org/10.1016/S1352-2310(98)00109-5

Nugent, A., & Decou, D. (2018). Chapter 5: Atmospheric Stability. In *Atmospheric Science*.

Phillips, N. G., Ackley, R., Crosson, E. R., Down, A., Hutyra, L. R., Brondfield, M., Karr, J. D., Zhao, K., & Jackson, R. B. (2013). Mapping urban pipeline leaks: Methane leaks across Boston. *Environmental Pollution*, *173*, 1–4. https://doi.org/10.1016/j.envpol.2012.11.003

*PRCI-REX2022-020_Jayarathne.pdf*. (n.d.). Retrieved August 30, 2023, from https://energy.colostate.edu/wp-content/uploads/sites/28/2022/12/PRCI-REX2022-020_Jayarathne.pdf

Riddick, S. N., Bell, C. S., Duggan, A., Vaughn, T. L., Smits, K. M., Cho, Y., Bennett, K. E., & Zimmerle, D. J. (2021). Modeling temporal variability in the surface expression above a methane leak: The ESCAPE model. *Journal of Natural Gas Science and Engineering*, *96*, 104275. https://doi.org/10.1016/j.jngse.2021.104275

Riddick, S. N., Mauzerall, D. L., Celia, M. A., Kang, M., Bressler, K., Chu, C., & Gum, C. D. (2019). Measuring methane emissions from abandoned and active oil and gas wells in West Virginia. *Science of The Total Environment*, *651*, 1849–1856. https://doi.org/10.1016/j.scitotenv.2018.10.082

Seinfeld, J. H., & Pandis, S. N. (2016). *Atmospheric Chemistry and Physics: From Air Pollution to Climate Change*. John Wiley & Sons.

Shadwick, E. H., Wilson, J. D., & Flesch, T. K. (2007). Forward Lagrangian stochastic simulation of a transient source in the atmospheric surface layer. *Boundary-Layer Meteorology*, *122*(2), 263–272. https://doi.org/10.1007/s10546-006-9114-0

Stull, R. B. (2015). *Practical Meteorology: An Algebra-based Survey of Atmospheric Science*. University of British Columbia. https://openlibrary-repo.ecampusontario.ca/jspui/handle/123456789/405

Tian, S., Smits, K. M., Cho, Y., Riddick, S. N., Zimmerle, D. J., & Duggan, A. (2022). Estimating methane emissions from underground natural gas pipelines using an atmospheric dispersion-based method. *Elementa: Science of the Anthropocene*, *10*(1), 00045. https://doi.org/10.1525/elementa.2022.00045

*USDOT Announces Bipartisan PIPES Act Proposal to Modernize Decades-Old Pipeline Leak Detection Rules, Invests in Critical American Infrastructure, Create Good-Paying Jobs, and Improve Safety | PHMSA*. (n.d.). Retrieved August 30, 2023, from https://www.phmsa.dot.gov/news/usdot-announces-bipartisan-pipes-act-proposal-modernize-decades-old-pipeline-leak-detection

*US-GHG-Inventory-2023-Main-Text.pdf*. (n.d.). Retrieved September 4, 2023, from https://www.epa.gov/system/files/documents/2023-04/US-GHG-Inventory-2023-Main-Text.pdf

Von Fischer, J. C., Cooley, D., Chamberlain, S., Gaylord, A., Griebenow, C. J., Hamburg, S. P., Salo, J., Schumacher, R., Theobald, D., & Ham, J. (2017). Rapid, Vehicle-Based Identification of Location and Magnitude of Urban Natural Gas Pipeline Leaks. *Environmental Science & Technology*, *51*(7), 4091–4099. https://doi.org/10.1021/acs.est.6b06095

Weller, Z. D., Hamburg, S. P., & Von Fischer, J. C. (2020). A National Estimate of Methane Leakage from Pipeline Mains in Natural Gas Local Distribution Systems. *Environmental Science & Technology*, *54*(14), 8958–8967. https://doi.org/10.1021/acs.est.0c00437

Weller, Z. D., Roscioli, J. R., Daube, W. C., Lamb, B. K., Ferrara, T. W., Brewer, P. E., & Von Fischer, J. C. (2018). Vehicle-Based Methane Surveys for Finding Natural Gas Leaks and

Estimating Their Size: Validation and Uncertainty. *Environmental Science & Technology*, acs.est.8b03135. https://doi.org/10.1021/acs.est.8b03135

Zannetti, P. (1990). *Air Pollution Modeling: Theories, Computational Methods and Available Software*. Springer US Imprint : Springer.

# 8 APPENDIX

## 8.1 A1 Parameters used in the modeling approach.

### *8.1.1 A1.1 Darcy's and Fick's law parameters*

*Table A1.1. Parameters used in Fick's and Darcy's law when applied to the ESCAPE$^{-1}$ model.*

| Parameter | Value |
|---|---|
| $F_d$ | $0.00185 m^3 s^{-1}$ |
| K | $1 \times 10^{-8}$ m $s^{-1}$ |
| $K_r$ | 0.2 |
| g | 9.8 m $s^{-2}$ |
| $\mu$ | $1.09\ 10^{-6}$ $m^2$ $s^{-1}$ |

### *8.1.2 A1.2 Classification of Atmospheric Stability*

Atmospheric stability is the tendency of the atmosphere to resist vertical motion. There are several ways of classifying atmospheric stability. Using Pasquill's measure of atmospheric stability, measurements in this study were classified based on wind speed and daytime insolation (Pasquill, 1961). Strong insolation represents sunny midday during midsummer in England while slight insolation corresponds to similar conditions in midwinter. Measurements in this study were taken during the day (between 10 am to 6 pm), therefore, the stability classes were considered based on daytime insolation. The wind speed during the experiments ranged from 0.7 to 5 m $s^{-1}$, hence, the data points were classified into PGSC A, B, C, and D (Tables A1.2).

*Table A1.2. Classification of atmospheric stability using the Pasquill Gifford Stability Classes (PGSC) based on wind speed (m $s^{-1}$) and daytime insolation (Pasquill, 1961). Strong insolation represents sunny midday during midsummer in England while moderate insolation corresponds to similar conditions in midwinter.*

| Stability class | Day | | | Night | |
|---|---|---|---|---|---|
| Wind speed (m $s^{-1}$) | Strong | Mod | Light | Overcast | Clear |
| <2 | A | A | B | | |
| 3 | B | B | C | E | F |
| 4 | B | C | C | D | E |
| 5 | C | C | D | D | D |
| >6 | C | D | D | D | D |

### *8.1.3 A1.3 Surface Roughness Length*

The surface layer model in WindTrax requires the surface roughness length ($z_0$, m), as one of the parameters to define the wind profile in a simulation. The roughness length is estimated based on the vegetation cover (Table A1.3). The rural testbed used in this study is covered by short grass, therefore a roughness length of 0.023 m was set during each simulation.

*Table A1.3. The roughness length of different surfaces is based on the vegetation cover of the site.*

| Surface Cover | Roughness Length, m |
|---|---|
| Sand | 0.0003 |
| Bare soil | 0.03 |
| Short grass | 0.023 |
| Tallgrass | 0.1 |
| Wheat | 0.15 |

### *8.1.4 A1.4 Monin-Obukhov Length*

When calculating a below-ground leak rate, the Monin-Obukhov length (L, m) which is the measure of atmospheric stability is estimated from the PGSC table (Tables A1.4).

*Table A1.4. Table for estimating the Monin-Obukhov length (L, m) based on the Pasquill-Gifford Stability class (PGSC)*

| PGSC | L(m) |
|---|---|
| A | -5.5 |
| B | -11 |
| C | -30 |
| D | 1E+17 |
| E | 30 |
| F | 11 |
| G | 5 |

## 8.2 A2 Instrument Calibration

The Remote Methane Leak Detector (RMLD; Heath Consultants Inc, Texas, USA) is an instrument that is often used by oil and gas company operators to screen and detect gas leaks. For this reason, the RMLD was calibrated alongside the Picarro G4302 gas analyzer (Picarro Inc, California USA) to validate the measurements. It has an operating range of 0 to 99, 999 ppm-m and a sensitivity of 10 ppm-m at 30 m (maximum path length). Further, before each experiment, the RMLD was self-tested (Section A2.1).

### *8.2.1 A2.1 RMLD Self-test*

The self-test is based on the procedure outlined by Heath Consultants Inc. (Heath, 2009). First, the controller is removed from the carrying case, and the trans receiver is left inside the carrying case. The RMLD is turned on and allowed to warm for 2 to 3 minutes. From the controller menu, use the SELECT button to scroll for the SELF-TEST icon. To initiate the self-test, the UP button in the menu is pressed. If the RMLD passes the self-test, the number 255 is displayed on the screen.

### *8.2.2 A2.2 RMLD Calibration*

The RMLD was calibrated by running it alongside the Picarro gas analyzer for 1.3 hours (Figure A2). The Picarro gas analyzer was used because it is a high-precision instrument (precision < 0.5 ppb). Gas was released at 10 standard liters per minute. The RMLD is an open-path Tunable Diode Laser (TDLAS) that averages $CH_4$ concentrations along the line-of-sight of the laser path. It reports $CH_4$ mixing ratios (in parts per million-meter) as a product of the average concentration, and the path length.

During calibration, the trans receiver was placed 2 m (path length) away from the source of the leak while the inlet of the Picarro was placed 0.5 m above the source (Figure A3.1). Measurements from the RMLD were converted to parts per million by dividing the mixing ratio by 2 m path length which allows for comparison with measurements from the Piccaro. One-minute averages of the data were obtained and used to derive the relationship between the two instruments.

From the result, the RMLD is not sensitive to low $CH_4$ concentrations (less than 5 ppm-m) as compared to the Picarro (Figure A2.1). When the values of $CH_4$ concentrations from the RMLD are plotted against values from the Picarro, a linear relationship is obtained with an $R^2 = 0.65$ and m=0.6227 (Figure A2.1). Measurements from the RMLD are divided by 0.62 as a correction factor.

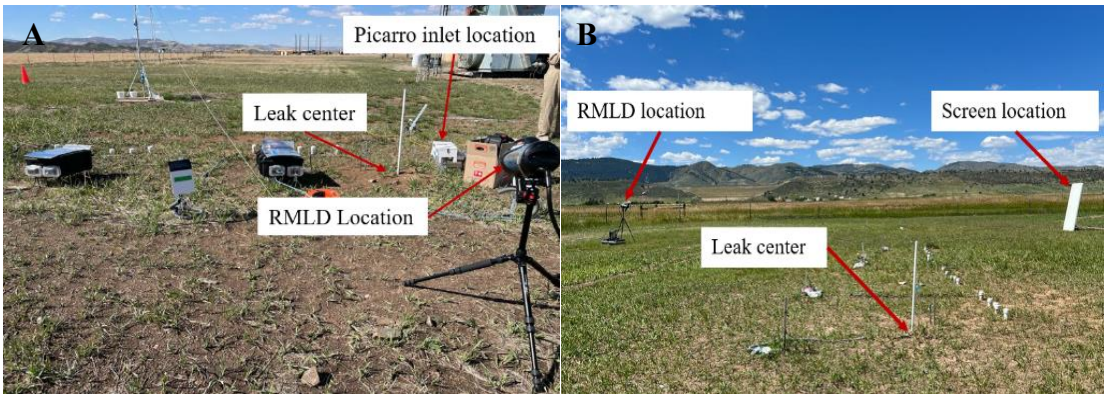


*Figure A2. The RMLD during calibration with the Picarro G4302 gas analyzer. A represents the setup of the RMLD during calibration, and B shows the set-up of the RMLD, and the reflective surface during above-ground downwind measurement.*

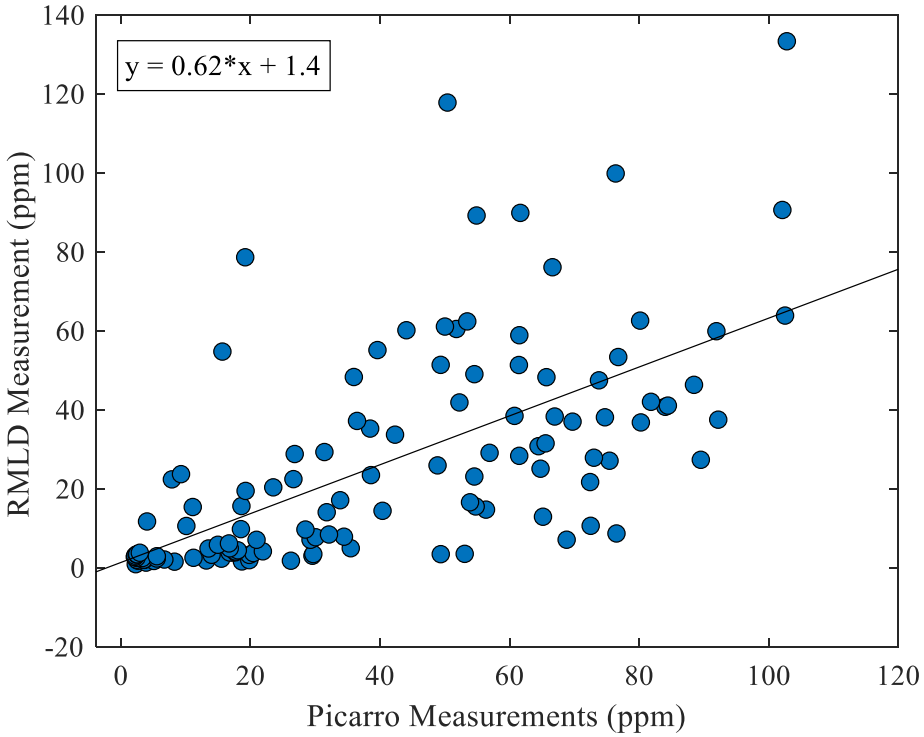


*Figure A2.1. Methane measurements from the RMLD versus Methane measurements from the Picarro. The plot shows a linear relationship between the measurements from the RMLD and measurements from the Picarro gas analyzer.*

**8.3 A3 Uncertainty Analysis**

The causes of uncertainty in this modeling approach are line averaged $CH_4$ mixing ratios measured by the RMLD, wind speed measurement, wind direction measurement, classification of atmospheric stability, and estimating the area of the surface expression of a leak.

The uncertainties are evaluated by performing a sensitivity analysis of the modeling approach in PG stability classes A, B, and C. 10-minute averaged $CH_4$ mixing ratios and meteorological data from the 0.4kg $h^{-1}$ controlled leak rate were used to perform the sensitivity analysis. Assuming that the individual uncertainties are inherent in the estimated leak rate, an uncertainty propagation was done to combine the uncertainties (S4.6).

The major steps in the sensitivity analysis are:

1. To derive surface emission using WindTrax's bLs model, and subsequently.
2. To derive a below-ground leak rate using the $ESCAPE^{-1}$ model.

3. To calculate the standard deviation (we use this to present uncertainty in each case) using the estimated leak rate in PG stability classes A, B, and C.

The calculated uncertainty from PG stability class B is used to present the uncertainty in the estimated leak rate (0.4kg $h^{-1}$ ± standard deviation in kg $h^{-1}$).

### *8.3.1 A3.1 Uncertainty due to Line-averaged $CH_4$ mixing ratios.*

The RMLD (Measurement Range: 0 to 99,9999 ppm-m, sensitivity: ± 5 ppm-m) is sold as a leak detection instrument, and as such, does not come with an estimate of accuracy in $CH_4$ mixing ratio measurement. To account for this, the RMLD was calibrated by running it alongside the Picarro gas analyzer (Section A2.2).

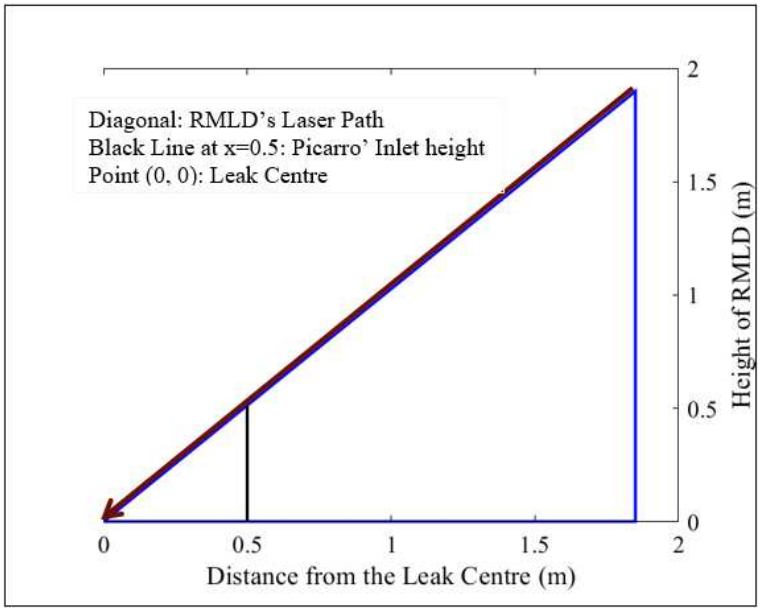


*Figure A3.1. Representation of the setup of the RMLD and Picarro during calibration. The RMLD was positioned such that the laser was located 2 m from the leak center. The Picarro was positioned 0.5m from the leak center. Methane readings were transmitted every 2 seconds in both instruments.*

To accurately quantify the accuracy of the RMLD, I used a Monte-Carlo bootstrap fit. A bootstrap fit involved randomly sampling RMLD measurements and Picarro measurements, with replacement to create multiple bootstrap samples. A total of 1000 bootstrap samples were used, for

each sample a linear regression model was fitted. From this, a 95% confidence interval of the slopes was calculated (Figure A3.1.1)

The lower bound and upper bound of the confidence interval were determined using the 2.5$^{th}$ and 97.5$^{th}$ percentiles of the bootstrap slopes, respectively (Figure 1). The mean, upper, and lower bound of the slopes from this sampling are 0.58, 0.74, and 0.45 respectively.

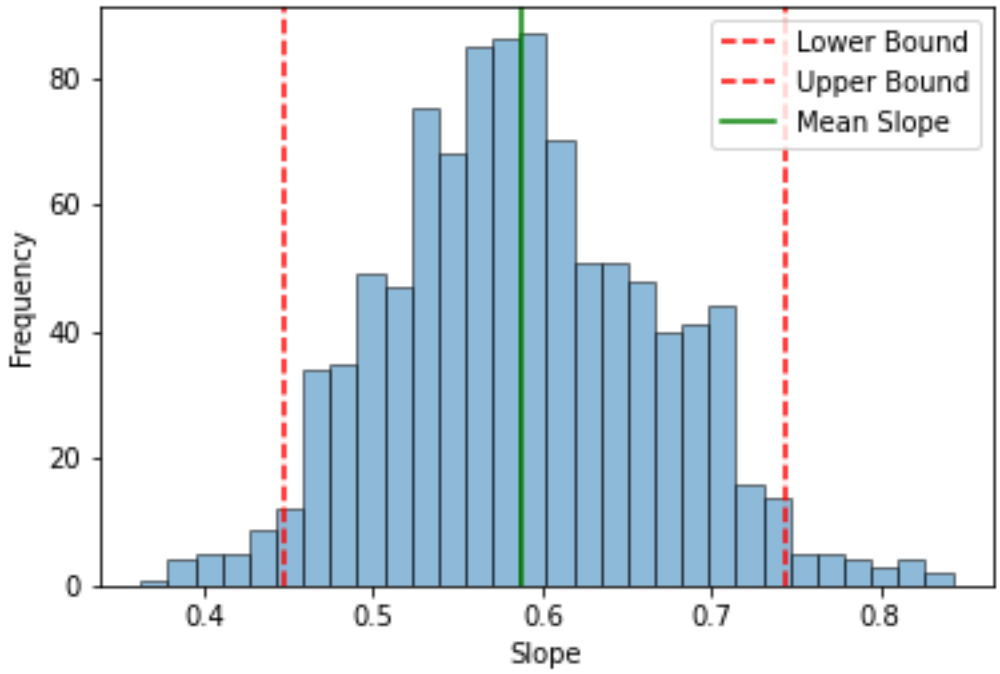


*Figure A3.1.1. Slopes obtained from bootstrap resampling (95% confidence interval: 0.43 to 0.74). Bootstrap resampling involved sampling RMLD measurements and the Picarro measurements, with replacement to create multiple linear regression models. A slope for each sample was then calculated. A 95 % confidence interval was derived by using slopes between the 2.5$^{th}$ to 97.5$^{th}$ percentiles. 0.45 represents the slope in the 2.5$^{th}$ percentile, while 0.74 represents the 97.5$^{th}$ percentile.*

Based on the analysis, the accuracy of the RMLD was derived using the mean, and the upper bound from the bootstrap fit (Equation 1). The accuracy is ±28%

$$R_U = \frac{Upper\ bound - Mean}{Mean} \qquad (1)$$

The uncertainty associated with the $CH_4$ mixing ratios was evaluated using the RMLD accuracy of $\pm 28\%$. The upper and lower bound of the $CH_4$ mixing ratios was obtained as $M_i \pm (0.28M_i)$,

where $M_i$ is the $CH_4$ mixing ratio. Input to WindTrax includes varied $CH_4$ mixing ratios, varied stability classes, constant area of the source, constant wind direction, constant wind speed, and constant downwind position of the RMLD. The surface emission rates were calculated in WindTrax and used to calculate subsurface leak rates in the ESCAPE[-1] model. A standard deviation was obtained for each PG stability class as $\sqrt{\frac{\sum_i^n (ELR_i - 0.4)^2}{(n-1)}}$, where ELR is the estimated leak rate and n is the number of data points in a stability class. Based on PG stability class B, the uncertainty associated with $CH_4$ mixing ratios is (0.40±0.20kg/h).

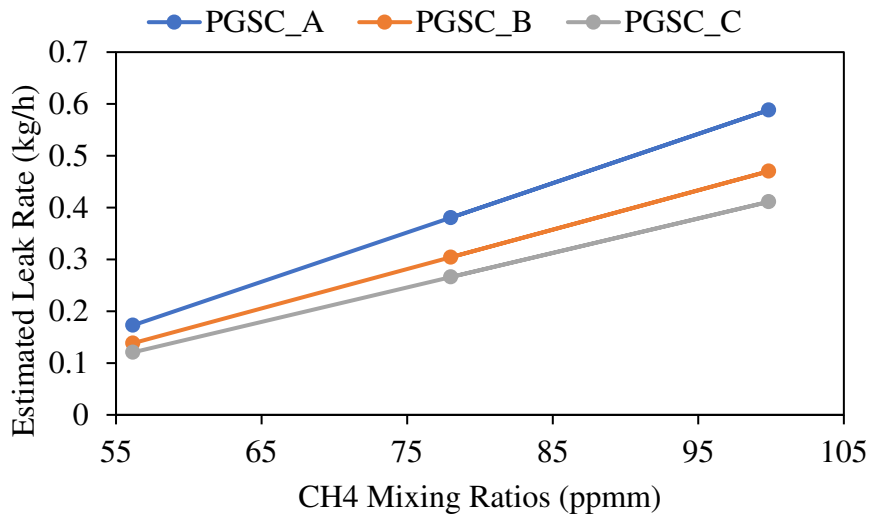


*Figure A3.1.2. The estimated leak rates are based on the RMLD accuracy of 28% in PG stability classes A, B, and C.*

### *8.3.2 A3.2 Uncertainty due to wind speed measurement*

To derive the surface emission, wind speed measurement is used as one of the inputs to WindTrax. Therefore, to assess the impact this might have on the estimated leak rate, a sensitivity analysis was done. The uncertainty associated with the wind speed measurements was evaluated using the sonic anemometer accuracy of $\pm 1\%$. The upper and lower bound of the wind speed was obtained as $WS_i \pm (0.01WS_i)$, where $WS_i$ is the wind speed measurement. Input to WindTrax includes varied wind speed, varied PGSC, constant area of the source, constant wind direction, constant $CH_4$ mixing ratios, and constant downwind position of the RMLD. The surface emission rates

were calculated in WindTrax and used to calculate the subsurface leak rates in the ESCAPE$^{-1}$ model. A standard deviation was obtained for each PG stability class as $\sqrt{\frac{\sum_i^n (ELR_i - 0.4)^2}{(n-1)}}$, where ELR is the estimated leak rate and n is the number of data points in a stability class. Based on PG stability class B, the uncertainty associated with wind speed is (0.4±0.07kg/h).

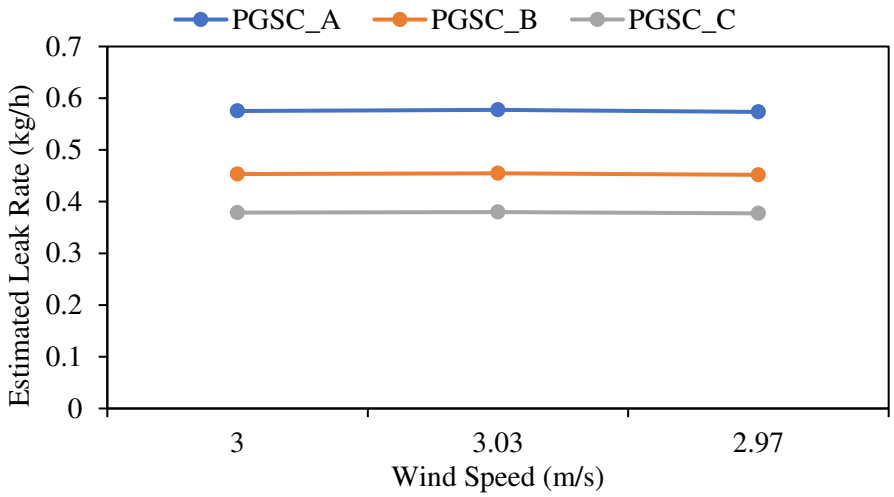


*Figure A3.2. The estimated leak rates are derived from varied wind speeds in PG stability classes A, B, and C.*

### *8.3.3 A3.3 Uncertainty due to wind direction measurement*

The wind direction determines the direction of flow of particles in the atmosphere, therefore, to calculate the surface emission in WindTrax, this was used as one of the inputs. To assess the impact the wind direction has on the estimated leak rate, an uncertainty analysis was done. The uncertainty associated with wind direction was calculated based on the sonic anemometer's accuracy of ±2°. The upper and lower bound of the wind direction was calculated as $WD_i \pm 2°$, where $WD_i$ is the wind direction measurement. Input to WindTrax includes varied wind direction, varied stability classes, constant area of the source, constant wind speed, constant $CH_4$ mixing ratios, and constant downwind position of the RMLD. The surface emission rates were calculated in WindTrax and used to calculate the subsurface leak rates in the ESCAPE$^{-1}$ model. A standard deviation was

obtained for each PG stability class as $\sqrt{\frac{\sum_i^n (ELR_i - 0.4)^2}{(n-1)}}$, where ELR is the estimated leak rate and n is the number of data points in a stability class. Based on stability class B, the uncertainty associated with wind direction is (0.4±0.03kg/h)

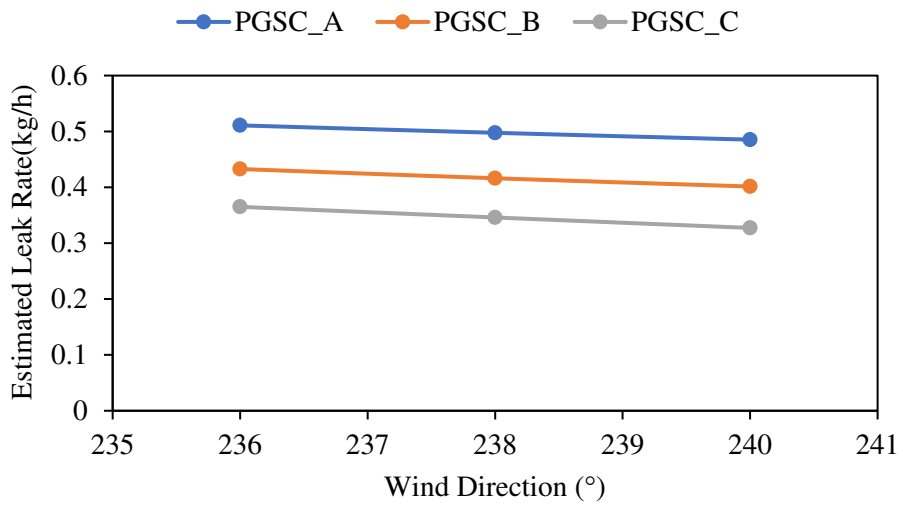


*Figure A3.3. The estimated leak rates derived from varied wind directions in PG stability classes A, B, and C.*

### *8.3.4 A3.4 Uncertainty due to classification of the Atmospheric Stability*

Atmospheric stability is the tendency of the atmosphere to resist the vertical motion of air parcels. Measurements in this study were classified into 3 different stability classes (A, B, C, D) based on wind speed and daytime insolation (Pasquill, 1961) (Table A1.2). PG stability class A represents Extremely unstable conditions, PG stability class B represents moderately unstable conditions and PG stability class C represents slightly unstable conditions. To illustrate the impact of this classification on the estimated leak rate, an uncertainty analysis was done.

In the uncertainty analysis, the PGSC was varied (A, B, C) while the wind speed, the wind direction, the area of the source, the $CH_4$ mixing ratios, and the downwind positioning of the RMLD were kept constant. The surface emission rates were calculated in WindTrax and used to calculate the subsurface leak rates in the ESCAPE$^{-1}$ model. A standard deviation was obtained as

$\sqrt{\frac{\sum_i^n (ELR_i - 0.4)^2}{(n-1)}}$, where ELR is the estimated leak rate and n is the number of data points. Based on this, the uncertainty associated with atmospheric stability is (0.4±0.12kg/h).

### *8.3.5 A3.5 Uncertainty due to the surface expression of a leak*

A below-ground leak forms an area source of emission on the surface. A study by Riddick et al., 2021 shows that gas migrates up to 4.5m from the leak center (the point directly above the leak). Therefore, to derive surface emissions in this modeling approach, we used a leak radius of 4 m. To illustrate the uncertainty associated with the surface expression of a leak, the radius of the area source was varied from 0.5 to 5m with 0.5m increments in WindTrax. The stability classes were varied but the wind direction, the $CH_4$ mixing ratios, and the downwind position of the RMLD were kept constant. The surface emission rates were calculated in WindTrax and used to calculate the subsurface leak rates in the ESCAPE$^{-1}$ model. A standard deviation was obtained for each PG stability class as $\sqrt{\frac{\sum_i^n (ELR_i - 0.4)^2}{(n-1)}}$, where ELR is the estimated leak rate and n is the number of data points in a stability class. Based on stability class B, the uncertainty associated with the surface expression of a leak is (0.4±0.15kg/h).

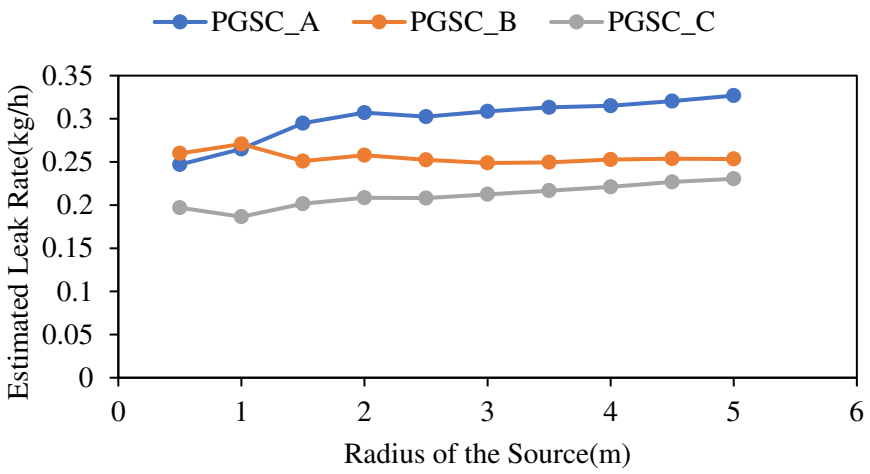


*Figure A3.5. The estimated leak rates are derived from varying the radius of the source from 0 to 5m in 0.5m increments. The estimated leak rates were calculated in PG stability classes A, B, and C.*

### *8.3.6 A3.6 Propagation of Uncertainty*

The uncertainty in the input data is propagated to the estimated below-ground leak rate. The estimated leak rate (ELR) in this approach is considered a function of changing line averaged $CH_4$ mixing ratios (M), changing wind speed (WS), changing wind direction (WD), the surface expression of a leak (Ar), and classification of atmospheric stability to PG stability classes A, B, and C. This is represented as ELR = f (M, WS, WD, Ar, A, B, C).

Using data from the 0.4 kg $h^{-1}$ leak, a linear model was used to correlate the estimated leak rate and the sources of uncertainty (Table A3.6). Each of the derivatives/estimates in each linear relationship was used to propagate the overall uncertainty (Equation 4.6). Based on the 0.4kg $h^{-1}$ leak, the overall uncertainty in the modeling approach is (0.4±0.10kg/h).

$$\sigma_{ELR}^2 = (\frac{\delta(ELR)}{\delta(M)})^2\sigma_M^2 + (\frac{\delta(ELR)}{\delta(WS)})^2\sigma_{WS}^2 + (\frac{\delta(ELR)}{\delta(WD)})^2\sigma_{WD}^2 + (\frac{\delta(ELR)}{\delta(A)})^2\sigma_A^2 + (\frac{\delta(ELR)}{\delta(P)})^2\sigma_P^2 \quad (3.6)$$

*Table A3.6. Derivatives and standard deviation of each source of uncertainty in the modeling approach. The product $d^2*V^2$ represents the derivative multiplied by the variance of each variable.*

| Variable | Derivative | Std (kg $h^{-1}$) | Derivative$^2$ ($d^2$) | Variance ($V^2$) | $d^2*V^2$ |
|---|---|---|---|---|---|
| M | 0.007 | 0.20 | 0.000049 | 0.04 | 0.000002 |
| WS | 0.117 | 0.07 | 0.014 | 0.0049 | 0.00007 |
| WD | -0.007 | 0.03 | 0.000049 | 0.0009 | 0.00000004 |
| Ar | -0.0024 | 0.15 | 0.0000058 | 0.023 | 0.0000001 |
| PG_A | -0.464 | 0.20 | 0.215 | 0.039 | 0.008 |
| PG_B | -0.262 | 0.15 | 0.069 | 0.021 | 0.0015 |
| PG_C | -0.12 | 0.16 | 0.014 | 0.026 | 0.0004 |
| | | | | Var (ELR) | 0.01 |
| | | | | Std (ELR) | 0.10 |

### 8.4 A4 Linear Relationships between the Variables and the Estimated Leak Rate

*8.4.1 A4.1 Methane Measurements and the Estimated Leak Rates*

Figure A4.1 shows the linear relationship between $CH_4$ mixing ratios (M), and the estimated leak rate.

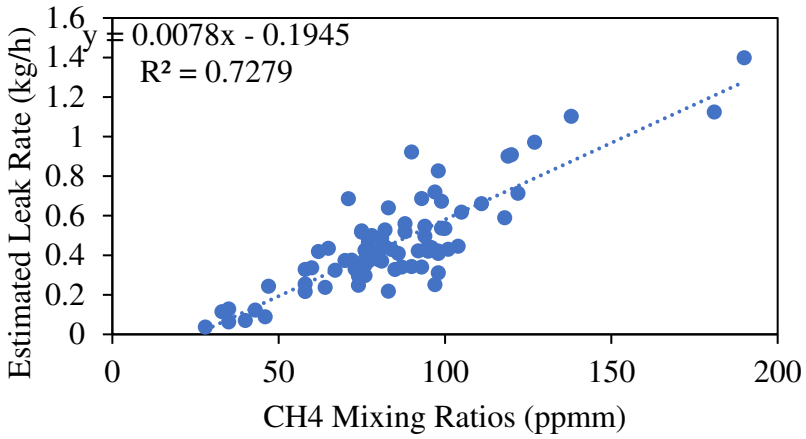


*Figure A4.1. A linear relationship between the estimated leak rate and Methane mixing ratios.*

*8.4.2 A4.2 Wind speed and the estimated leak rates*

Figure A4.2 shows a linear relationship between wind speed and the estimated leak rate.

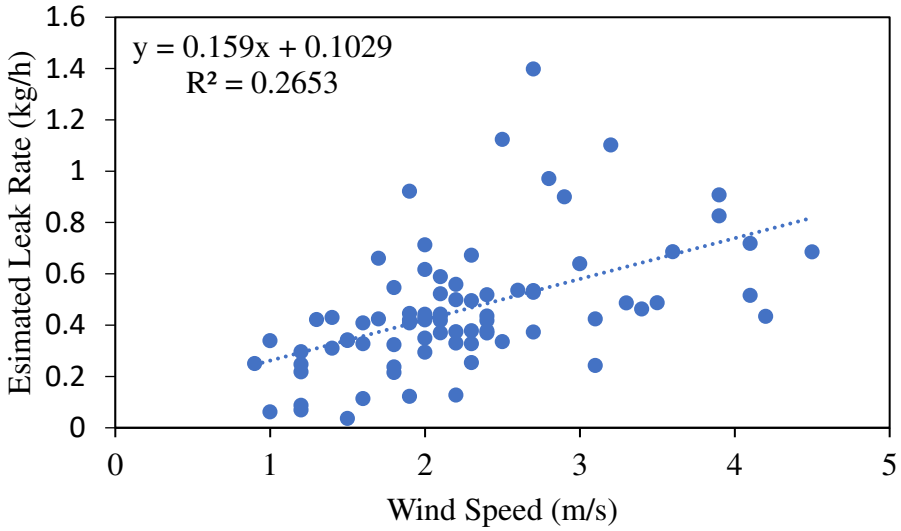


*Figure A4.2. A linear relationship between the estimated leak rate and wind speed*

*8.4.3 A4.3 Wind direction and the estimated leak rates*

Figure A4.3 below shows a linear relationship between the wind direction and the estimated leak rate.

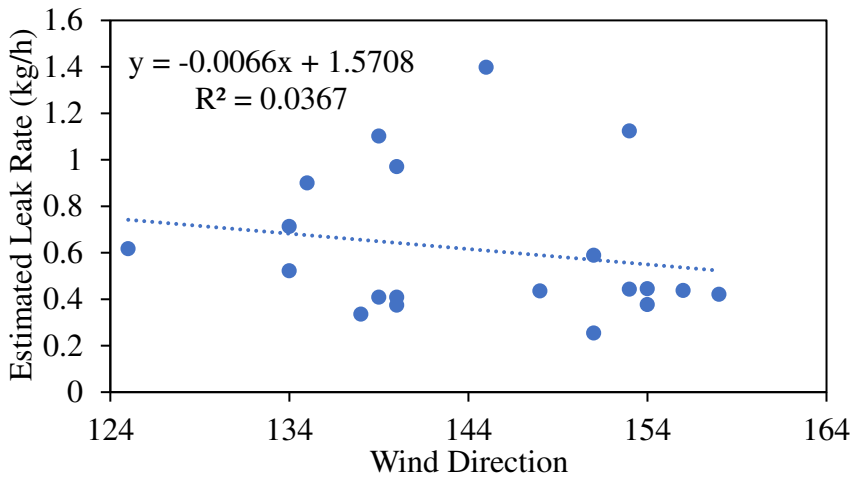


*Figure A4.3. A linear relationship between the estimated leak rate and wind direction*

### *8.4.4 A4.4 Area of the source and the estimated leak rates*

When deriving the surface emission in WindTrax, the radius of the source was constantly considered as 4m. Therefore, using this to establish a relationship with the estimated leak rate was not possible. To establish a linear relationship with the estimated leak rate, the results of section A3.5 were used. Figure A4.4 shows a linear relationship between the radius of the source and the estimated leak rate.

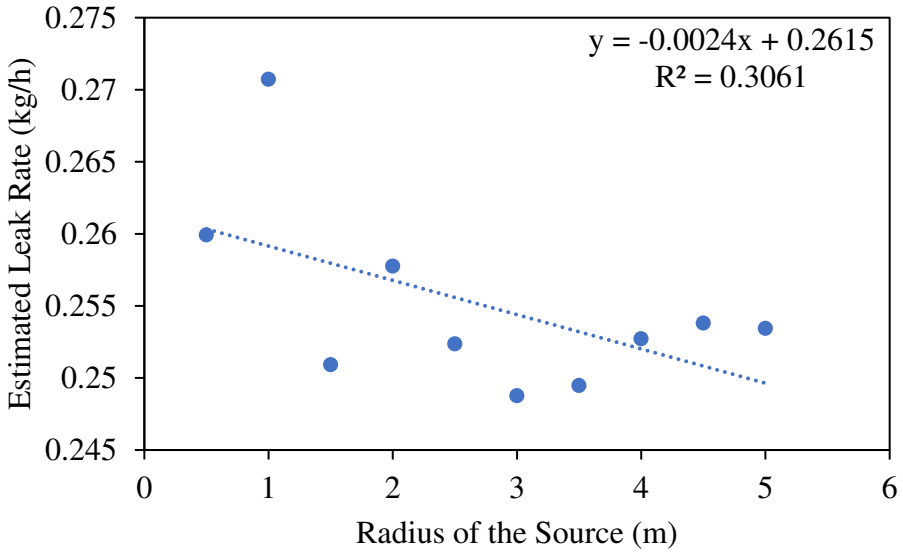


*Figure A4.4. A Linear relationship between the estimated leak rate and the radius of the source*

### 8.5 A5 Above-ground Plume

In this study, a line-averaging sensor was used to take above-ground $CH_4$ measurements. This means that to obtain reliable measurements, the sensor should be set up downwind and perpendicular to the wind direction. The essence of this setup is to ensure that the sensor is averaging across the plume centerline. A plume centerline is the center of mass of gas particles i.e., high concentration of particles (Figure A5). From the centerline, the concentrations of gas particles decrease (to approximately 10% of the concentrations at the centerline) as you move toward the plume edge (Stull, 2015).

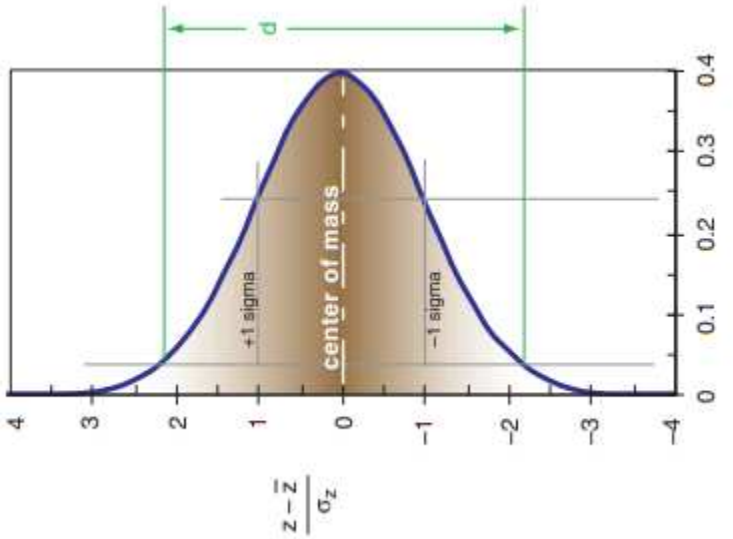


*Figure A5. Dispersion of gas in the atmosphere from the plume 'centerline' (Centre of mass, Stull (2015)*

The modeling approach in this study was biased when the wind direction changed rapidly. This is because the change in wind direction shifts the gas plume and makes the sensor measure either along the plume centerline or at the plume edge. If measuring along the plume centerline, then it is measuring high concentrations. If measuring at the plume edge, then it is measuring low concentrations of methane. Measuring from either the plume centerline or the plume edge biases the below-ground estimated leak rate (overestimates or underestimates, respectively).

### 8.6 A6 Wind Speed and Wind Direction

Figure A6 shows wind speeds and their respective wind direction for the experiments conducted.

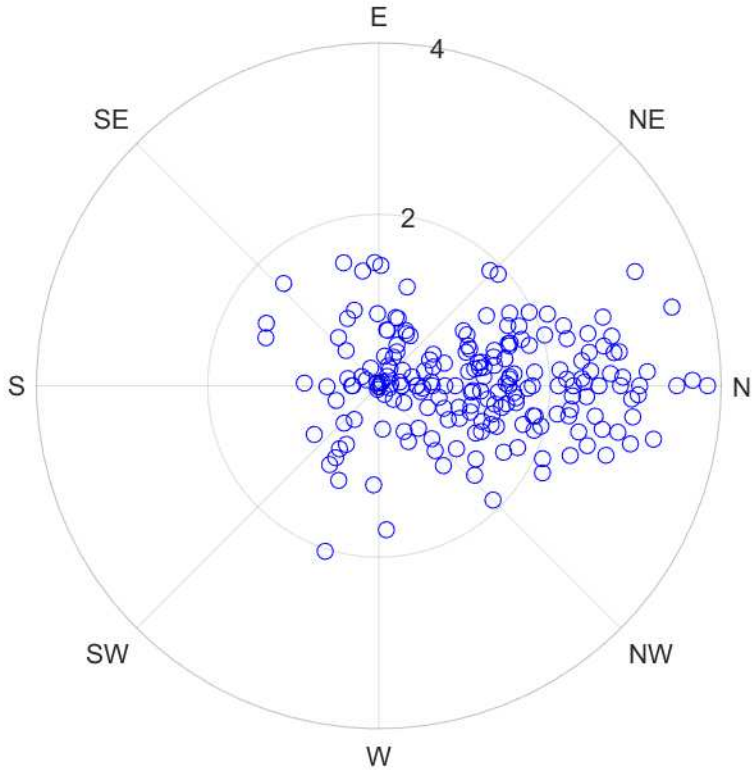


*Figure A6. Wind speed rose for the METEC facility between September and December 2021. Wind speed ranged from 0.7 to less than 5 m $s^{-1}$. Measurements in this plot were binned by 1 m $s^{-1}$ wind speed.*

### 8.7 A7 Temperature and Relative Humidity

Results of a Pearson's correlation test show that temperature and relative humidity do not have a linear correlation with the estimated leak rate (Table A7).

*Table A7. Correlation between the environmental variables, i.e., temperature and relative humidity with the estimated leak rate.*

| | p-value | $R^2$ | m |
|---|---|---|---|
| Temperature | <0.05 | 0.1043 | -0.0120 |
| Relative Humidity | <0.05 | 0.0148 | 0.0020 |